

MIT Open Access Articles

Understanding Continuous Lithium-Mediated Electrochemical Nitrogen Reduction

The MIT Faculty has made this article openly available. **Please share** how this access benefits you. Your story matters.

Citation: Lazouski, Nikifar et al. "Understanding Continuous Lithium-Mediated Electrochemical Nitrogen Reduction." *Joule*, 3, 1, (April 2019): 916-916 © 2019 Elsevier Inc.

As Published: <http://dx.doi.org/10.1016/j.joule.2019.02.003>

Publisher: Elsevier BV

Persistent URL: <https://hdl.handle.net/1721.1/123849>

Version: Author's final manuscript: final author's manuscript post peer review, without publisher's formatting or copy editing

Terms of use: Creative Commons Attribution-NonCommercial-NoDerivs License



Understanding Continuous Lithium-Mediated Electrochemical Nitrogen Reduction

Nikifar Lazouski,¹ Zachary J Schiffer,¹ Kindle Williams,¹ and Karthish Manthiram^{1*}

¹Department of Chemical Engineering; Massachusetts Institute of Technology; Cambridge, MA
02139, USA

*Corresponding Author: karthish@mit.edu

Summary

Ammonia is a large-scale commodity chemical that is crucial for producing nitrogen-containing fertilizers. Electrochemical methods have been proposed as renewable and distributed alternatives to the incumbent Haber-Bosch process, which utilizes fossils for ammonia production. Herein, we report a mechanistic study of lithium-mediated electrochemical nitrogen reduction to ammonia in a non-aqueous system. The rate laws of the main reactions in the system were determined. At high current densities, nitrogen transport limitations begin to affect the nitrogen reduction process. Based on these observations, we developed a coupled kinetic-transport model of the process, which we used to optimize operating conditions for ammonia production. The highest Faradaic efficiency observed was $18.5 \pm 2.9\%$, while the highest production rate obtained was $(7.9 \pm 1.6) \times 10^{-9} \text{ mol cm}^{-2} \text{ s}^{-1}$. Our understanding of the reaction network and the influence of transport provides foundational knowledge for future improvements in continuous lithium-mediated ammonia synthesis.

Introduction

Ammonia is one of the most widely produced industrial chemicals, with a worldwide production of 170 million tons per annum.¹ At least 80% of ammonia is used in fertilizer production, making ammonia production critical for agriculture.² Today, ammonia is produced predominantly via the Haber-Bosch process, which involves reacting nitrogen and hydrogen over heterogeneous catalysts at high temperatures of 450-500°C and pressures up to 200 atm.³ Hydrogen gas is typically generated on-site from fossil fuels via steam reforming; this leads to significant carbon dioxide emissions of 1.9-9.3 tons CO₂ per ton of NH₃.^{4,5} In total, the Haber-Bosch process consumes approximately 1% of the world's energy supply and emits over 450 million tons of CO₂ per year.^{4,6} Because of the harsh operating conditions and on-site hydrogen production, the process is economically viable only at large scales.⁷ This makes it difficult to produce ammonia in a modular and distributed manner through Haber-Bosch. Distributed ammonia production, if achieved, could reduce inefficiencies and costs associated with fertilizer distribution.⁸

In order to overcome these challenges, methods to produce ammonia electrochemically from nitrogen and water at ambient conditions have been proposed, which could help to reduce the CO₂ footprint of the process. Operating at ambient conditions without the use of steam reforming enables smaller scale processes with lower capital costs.⁹ The reduced CO₂ footprint and capital costs, as well as the economics associated with distributed production, can make electrochemical reduction competitive with industrial Haber-Bosch in certain contexts. Many catalyst chemistries have been proposed for electrochemical nitrogen reduction, including structured noble metals,¹⁰ metal oxides,¹¹ metal nitrides,¹² metal sulfides,¹³ nitrogen- and boron-doped carbon,¹⁴ and lithium metal.¹⁵⁻¹⁹ Despite the large variety of reported catalysts, many of

them exhibit low Faradaic efficiencies (FEs) and rates for producing ammonia, often below 10% and 10^{-10} mol cm⁻² s⁻¹, respectively (Table S1).^{19,20}

Among these chemistries, lithium metal-based methods report some of the highest FEs (Table S1).^{15–18} Lithium metal is unique in that it can undergo a bulk reaction in which it spontaneously splits the nitrogen triple bond at ambient conditions.²¹ In lithium-mediated nitrogen reduction, lithium ions are reduced to lithium metal, which spontaneously reacts with nitrogen to form lithium nitride. The lithium nitride then reacts with a proton source to form ammonia. High FEs in lithium-mediated nitrogen reduction were often achieved by running the process in a batchwise fashion,^{16–18} at elevated pressures,¹⁵ or at elevated temperatures at certain steps.^{16,18} It would be attractive to produce ammonia continuously at ambient temperatures and pressures. In this vein, a continuous method has been reported in which lithium metal is plated onto metal electrodes from a 0.2 M lithium perchlorate, 1% ethanol in tetrahydrofuran solution in the presence of nitrogen to produce ammonia.¹⁵ However, mechanistic understanding of this process is lacking, which makes it difficult to rationally improve the process yields.

Herein, we report a mechanistic study of continuous lithium-mediated ammonia production at room temperature and pressure. We determined the rate laws of the two main rate-limiting reactions in the system: the reaction between lithium and ethanol to form hydrogen (lithium protolysis) and the reaction between lithium and nitrogen to form lithium nitride (lithium nitridation), from which ammonia is evolved. These rate laws were integrated into a coupled kinetic-transport model that incorporated the competing reactions in a simple reaction network. The model is able to explain experimental results with great fidelity. The model also suggests that transport limitations can be observed in the system for nitrogen reduction, demonstrating the fast intrinsic kinetics of the lithium-mediated approach. Through a series of improvements in

experimental setup, including utilization of a separator, drying of solvents, purification of reagents, and galvanostatic operation, and through mechanistic understanding of the process, we obtained high ammonia FEs and rates at ambient conditions. The maximum FE and production rate obtained were $18.5 \pm 2.9\%$ and $7.9 \pm 1.6 \times 10^{-9} \text{ mol cm}^{-2} \text{ s}^{-1}$, respectively.

Results

Electrochemical Approach

The lithium-mediated nitrogen reduction cycle was run continuously in a 2-compartment electrochemical cell (Figure 1, S1, S2). In this setup, lithium metal is plated onto an inert metal substrate from solution in a polar, aprotic solvent. Nitrogen gas dissolved in the electrolyte reacts with the plated lithium to form lithium nitride. The nitride reacts with the proton carrier, here ethanol, to form ammonia that remains dissolved in the electrolyte.

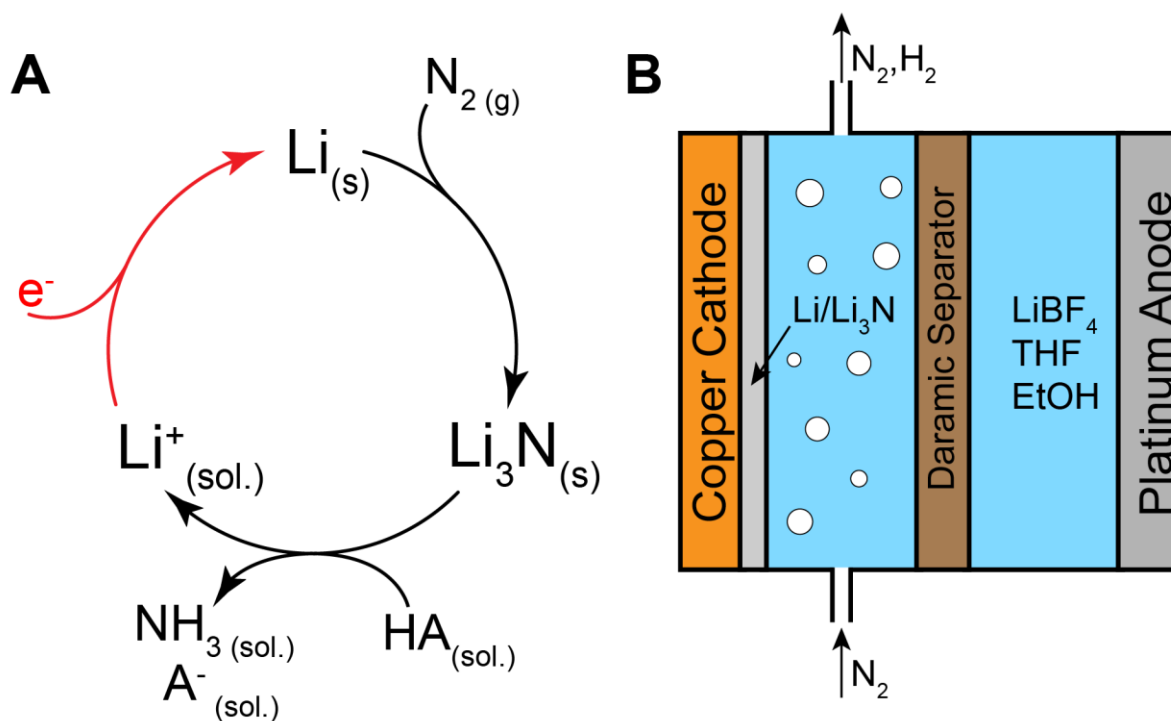


Figure 1. Lithium-mediated nitrogen reduction to ammonia. (A) The chemistry involved in ammonia synthesis. Compound subscripts denote phases; (s) is solid, (g) is gas, (sol.) is solution phase. (B) The electrochemical cell setup used in the described experiments.

Control Experiments

It is imperative to verify that detected ammonia is a result of N₂ reduction and does not originate from either adventitious sources or contaminants.^{4,22} We performed a series of control experiments in order to confirm N₂ reduction (Figure 2). The concentration of ammonia in the cell was found to increase with time when applying a constant current, as determined by taking periodic aliquots from a single operating cell (Figure 2A), which supports the assertion that ammonia is generated during electrolysis and is not present as a contaminant before the experiment. As HNO₃ is used in preparing the cathode (see SI Experimental Procedures), we sought to rule out nitrate reduction as the source of ammonia. When HCl-etched and unetched copper foils were used as the cathode, ammonia is still detected, confirming that contamination from HNO₃ etching is not responsible for ammonia formation (Figure S6). When argon was used as the feed gas, little ammonia was detected (Figure 2B); the ammonia that was detected in this argon control was likely produced due to residual nitrogen in the cell (see SI Experimental Procedures). This confirms that the presence of dinitrogen is required for ammonia generation.

Isotopic labeling of nitrogen allowed us to directly trace conversion of dinitrogen to ammonia.^{4,23–26} When isotopically labelled nitrogen gas, ¹⁵N₂, was used as the feed gas, ammonia was first detected via the colorimetric assay (Figure 2B, S3, S4, S5), then analyzed by NMR. When ¹⁴N₂ was used as the feed gas, a triplet with equal peak intensities was observed at 7.23 ppm with $J = 52.2$ Hz, corresponding to ¹⁴N-¹H coupling in NH₄⁺ (Figure 2C).²⁷ The NMR spectrum of the electrolyte solution obtained following electrolysis of ¹⁵N₂ contains a doublet at 7.23 ppm with $J = 73.2$ Hz, corresponding to ¹⁵N-¹H coupling in NH₄⁺ (Figure 2C),²⁷ which confirms that ammonia was made from the feed ¹⁵N₂. As ammonia contamination of isotopically labeled nitrogen feedstocks is possible,^{28,29} we performed additional control experiments in which both ¹⁵N₂ and

$^{14}\text{N}_2$ were fed to the cell in the absence of polarization. No ammonia was detected in either case by NMR or colorimetric assay, confirming the purity of the gas feeds, and further validating that ammonia was formed via nitrogen reduction.

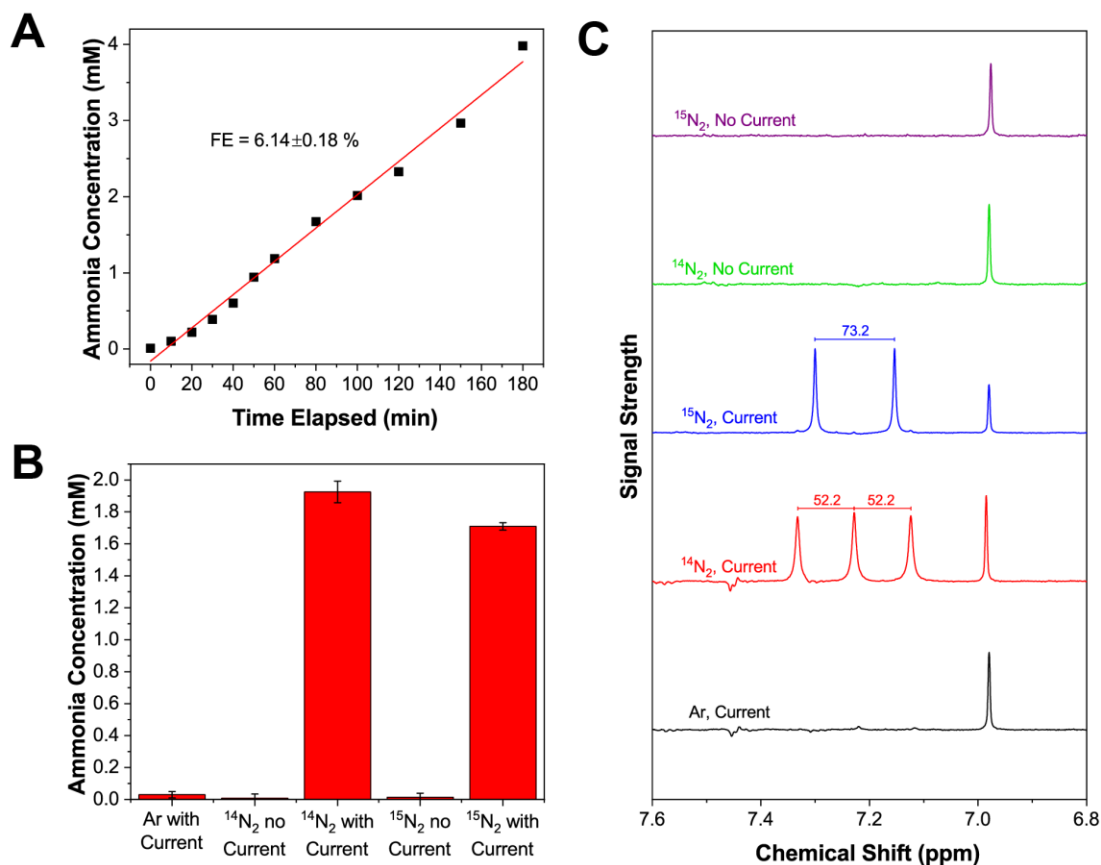


Figure 2. Control experiments confirming ammonia generation via nitrogen reduction. (A) Evolution of ammonia concentration over time in a cell containing 0.2 M EtOH and an applied current density of 3 mA cm^{-2} . (B) Concentrations of ammonia in the electrolyte solutions following experiments in which $^{15}\text{N}_2$, $^{14}\text{N}_2$, and Ar were used as feed gases as measured by the colorimetric assay. A 15 mA cm^{-2} current was applied for 15 minutes in experiments with current; no current was applied for the same amount of time in the other experiments. Error bars depict the standard deviation in the quantification assay based on $n=2$. (C) NMR spectra of the solutions from aforementioned experiments. The $^{15}\text{N}_2$ plot has been scaled down relative to the other spectra for readability. The different proton splitting patterns spectra resulting from $^{14}\text{N}_2$ and $^{15}\text{N}_2$ gas feeds support the claim that ammonia comes from the feed gas.

Effect of Nitrogen Concentration on Nitrogen Reduction

As nitrogen is the species that is being reduced, we sought to understand the impact of nitrogen partial pressure on the observed FE towards ammonia. The partial pressure of nitrogen was varied between 0 and 1 bar by diluting the nitrogen stream with argon; the concentration of ethanol in the system was kept constant at 0.2 M and a constant current of 3 mA cm⁻² was applied to produce ammonia. The FE towards ammonia increased linearly with nitrogen pressure (Figure 3). As nitrogen concentration in solution is proportional to the partial pressure of nitrogen due to Henry's law, we can conclude that the reaction between lithium and nitrogen is first order in nitrogen. The partial current density towards ammonia in these experiments is significantly lower than the transport-limited current density (see Supplemental Information), which implies that the first-order behavior is a manifestation of the kinetics of the process, not the transport. The fact that ammonia yields decrease at lower partial pressures of nitrogen helps to further validate that ammonia comes from nitrogen reduction and not from adventitious sources.

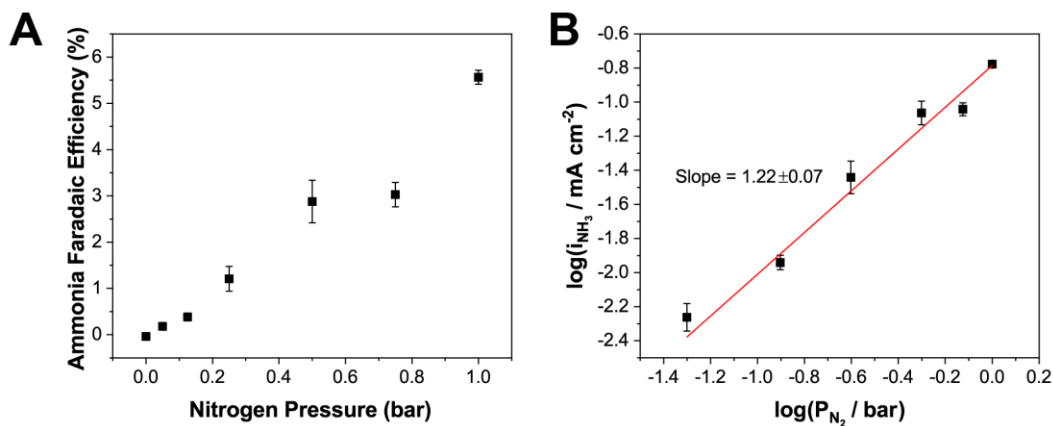


Figure 3. Effect of nitrogen partial pressure on ammonia production. Variation in (A) Faradaic efficiency and (B) production rate towards ammonia with varying partial pressures of N₂. The partial pressure was controlled by diluting N₂ with Ar. When no N₂ was present, no ammonia was detected. Error bars represent the standard deviation between replicates of the same experiment with n = 3.

Effect of Proton Carrier Concentration

We elucidated the effect of the proton carrier, ethanol, by varying its concentration while holding the nitrogen pressure and current density constant at 1 bar and 3 mA cm⁻², respectively. No ammonia or hydrogen was generated in the absence of ethanol, and a significant layer of lithium accumulated on the surface of the cathode (Figure S7); this implies that the applied current goes towards plating lithium which remains unreactive in the absence of ethanol. The ammonia FE initially increases with increasing ethanol concentration and reaches a peak value at 0.1 M, with an average Faradaic efficiency towards ammonia of $7.8 \pm 3.0\%$ (Figure 4A, Table S4). At ethanol concentrations >0.1 M, the Faradaic efficiency for ammonia decreases monotonically with ethanol concentration; the main side product under these conditions is hydrogen gas (Figure S15). The rate of ammonia generation exhibits an approximately -1.5 order with respect to ethanol concentration in this regime (Figure 4B). We believe this effect can be explained by a decrease in the amount of lithium available for nitridation at higher ethanol concentrations due to increased competition from direct lithium protolysis by ethanol; this is reflected in the lower coverage of lithium at higher ethanol concentrations (Figure S7A-C).

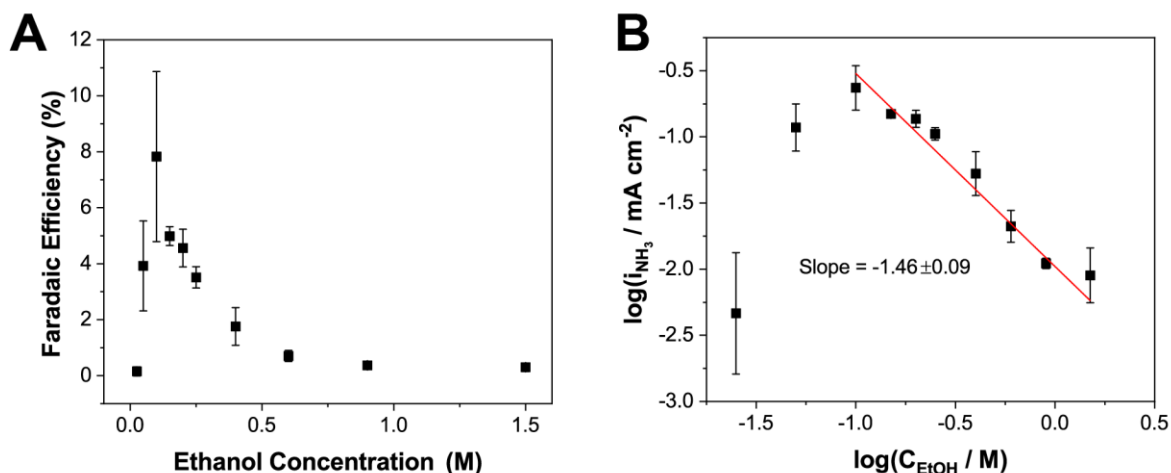


Figure 4. Effect of ethanol concentration on ammonia production. The effect of varying ethanol concentration on (A) the Faradaic efficiency and (B) production rate of ammonia. There is an optimal ethanol concentration at which ammonia yields are maximized. At higher concentrations, ethanol competes with nitrogen to react with lithium, which leads to a negative order with respect to ethanol, as seen in (B). Error bars represent the standard deviation between replicates of the same experiment with $n = 3$.

It is important to address the economic and practical aspects of using ethanol as a proton carrier for ammonia synthesis. We define the proton carrier to be the species that protonates lithium and lithium nitride in the reactions at the cathode, while the hydrogen source is the species that loses hydrogen atoms in the overall reaction at both electrodes. In this study, ethanol is used as a model proton carrier that can lead to high ammonia yields while forming lithium ethoxide; it is also the hydrogen source. While ethanol is a renewable hydrogen source, as it is produced from biomass, it is not economically viable to use ethanol as the hydrogen source for ammonia synthesis at industrial scales. It would be desirable to use water instead of ethanol as the hydrogen source due to its lower cost. Adding water to the catholyte was found to negatively affect ammonia yields, which may hinder its use as a direct proton source and carrier (Figure S9). In future work, one way to utilize water as the hydrogen source could be by oxidizing it at the anode to produce oxygen gas and protons; the protons could react with free proton carrier and be transported to the cathode

(Figure S17). Alternatively, hydrogen gas sourced from water-splitting could be oxidized at the anode. In both of these setups, ethanol, or any other chosen carrier molecule, would only act as the proton carrier to the cathode and would not be consumed.

Effect of Current Density

In order to study the effect of the rate of lithium plating on the production of ammonia, the applied current density was varied between 0.3 mA cm^{-2} and 25 mA cm^{-2} . The concentration of ethanol in these experiments was held constant at 0.2 M, a concentration higher than the optimal one. This value was chosen in order to maintain a low surface concentration of the plated lithium, which is useful for mechanistic analysis (see Discussion), as well as to obtain results with less variation in FE between runs, since the standard deviation in FE is smaller at ethanol concentrations higher than the optimal one. The FE and rate of ammonia production change significantly with applied current density. The rate for ammonia production increases monotonically with increasing current density (Figure 5C). This implies that the nitride formation rate increases with current density; this is consistent with previously reported observations of faster nitrogen fixation in Li-ion batteries at increased plating current densities.³⁰ The FE towards ammonia, however, increases with current density only at low current densities (Figure 5A). In this region, the FE increases proportionately to the square root of current density. At approximately 15 mA cm^{-2} , the FE reaches a maximum value, with an average FE of $8.6 \pm 2.2\%$. At higher current densities, the FE towards ammonia begins to decrease. We believe that the peak in FE is caused by nitrogen transport limitations, as discussed below.

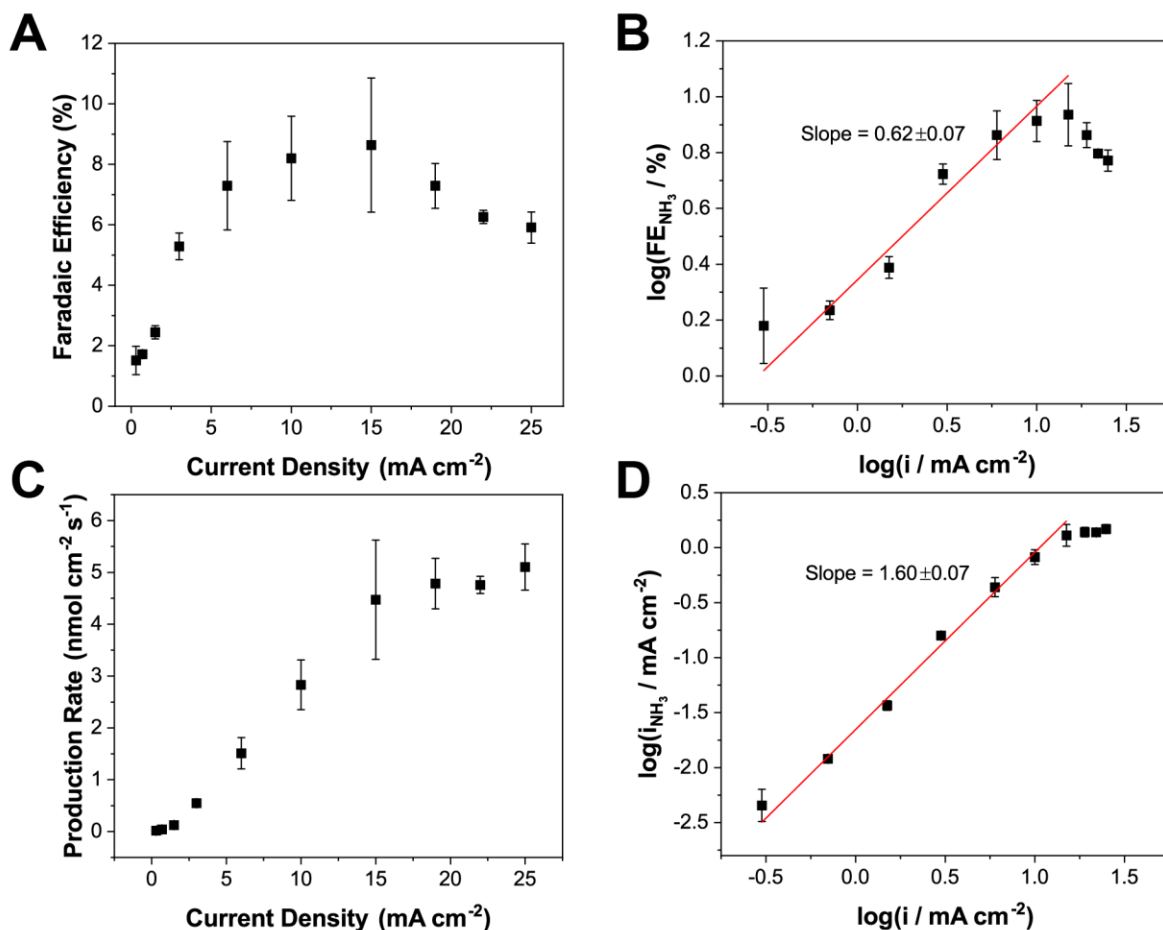


Figure 5. Effect of applied current density on ammonia production. The effect on (A, B) Faradaic efficiency and (C, D) production rate. Initially, the FE increases proportionally to the square root of the current density. At approximately 15 mA cm^{-2} , the FE peaks and begins to decrease. The production rate monotonically increases with current density, but begins to stabilize above 15 mA cm^{-2} . Error bars represent the standard deviation between replicates of the same experiment with $n = 3$.

Discussion

The existence of an optimal ethanol concentration at which ammonia production is maximized reveals many mechanistic details of ammonia synthesis (Figure 4). The negative order with respect to ethanol at higher ethanol concentrations can be explained by competition between nitrogen and ethanol for reacting with lithium metal and will be discussed in more detail below through our mechanistic model. The reasons for the positive order in ethanol at low concentrations

are less obvious, however. One potential explanation could be that at low concentrations of ethanol, there is insufficient ethanol to protonate lithium nitride that forms when nitrogen reacts with lithium, which leads to accumulation of lithium nitride. Accumulation of material on the cathode surface (Figure S7A) and low hydrogen FEs (Figure S15) at low ethanol concentrations support this hypothesis. However, after dissolving the residual solids in 0.1 M HCl following electrolysis, insignificant amounts of ammonia were detected in the resulting solution (Figure S12). If lithium nitride were present, rapid protolysis by HCl would produce large amounts of ammonia. This suggests that the solids do not contain lithium nitride; instead, they most likely contain unreacted lithium.

Alternatively, at low ethanol concentrations, increasing the ethanol concentration may assist nitride formation. This could occur if higher ethanol concentrations disrupt the solid-electrolyte interphase (SEI) on the lithium.³¹ This would expose more fresh lithium for reactions. Another mechanism by which ethanol could assist nitride formation is by causing defects in the structure of lithium. A similar effect has been observed in solid state lithium nitridation, wherein the reaction is accelerated in the presence of small amounts of water vapor.³² In this case, water vapor acts as a proton source and creates defects at which nitrogen can react.³² Regardless of the mechanism, increases in ethanol concentration promote reactions between lithium and both ethanol and nitrogen, leading to significantly higher ammonia and hydrogen FEs (Figure 4, S15) than observed in the absence of ethanol.

At high ethanol concentrations, a great deal of mechanistic insight can be extracted from the order of the ammonia production rate with respect to nitrogen and ethanol, as well as from the dependence of FE on current density. In particular, the observed orders with respect to current density and ethanol are non-integer, which implies interactions between elementary reactions. In

order to explain the observed phenomena, we developed a model that describes the reactions of plated lithium with nitrogen or ethanol to form ammonia or hydrogen, respectively. We assume that there is a small amount of lithium on the surface that is constant in time, but can change with operating conditions. This amount is assumed to be significantly lower than the equilibrium amount of lithium defined by the applied potential; the amount is instead defined by the competing lithium formation and consumption reactions after an initial plating time, and can be found by invoking a quasisteady-state approximation (QSSA) for lithium.³³ The amount of lithium per geometric surface area, which is similar to a surface concentration, is denoted by $[Li]$. The assumption of low surface concentration is justified by the associated assumption of high ethanol concentration (Figure S7). The reactions with lithium have rates proportional to the lithium concentration to some power:

$$r_{H_2} = k_1 [Li]^\alpha [EtOH]^x \quad (1)$$

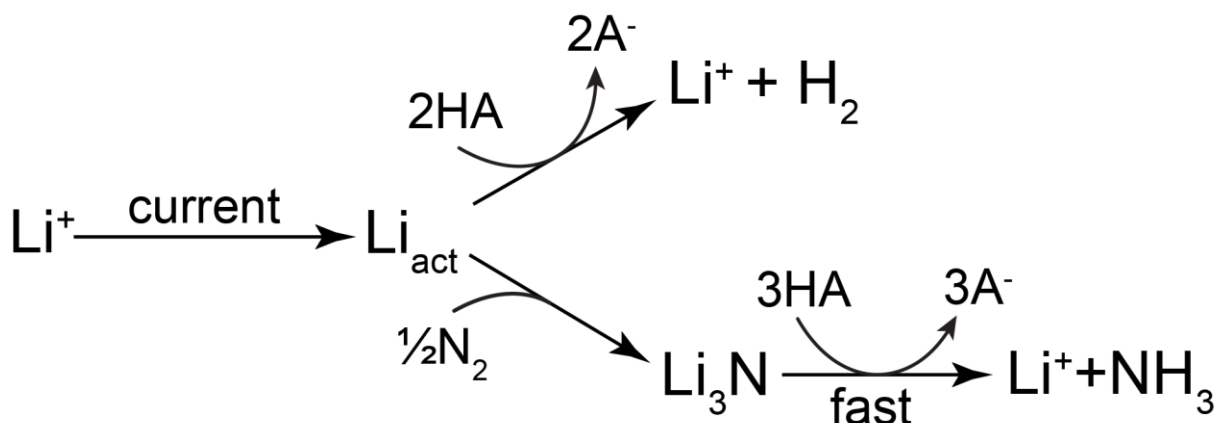
$$r_{NH_3} = k_2 [Li]^\beta [N_2] \quad (2)$$

Here, the rate constants k_1, k_2 are defined to result in rates in units of current density, i.e. they contain Faraday's constant F and any proportionality constants derived from stoichiometry. The rate constants are assumed to be independent of applied current or potential as they describe thermochemical reactions. $[N_2]$ and $[EtOH]$ are the concentrations of nitrogen and ethanol at the electrode surface, respectively. We assume the nitridation reaction is first order in nitrogen from the measured nitrogen partial pressure data (Figure 3). While this reaction formally generates lithium nitride (Li_3N), we assume that the lithium nitride protolysis reaction is fast, such that the reaction between lithium and nitrogen is rate-limiting. This assumption is supported by a lack of lithium nitride observed in the solids on the cathode after electrolysis (Figures S7, S12). In

addition, to simplify the analysis, we assume that the rate of the ammonia forming reaction is significantly lower than the rate of the hydrogen forming reaction:

$$k_2[Li]^\beta[N_2] \ll k_1[Li]^\alpha[EtOH]^x \quad (3)$$

This assumption is valid as the partial current towards ammonia is approximately an order of magnitude lower than the partial current towards hydrogen at ethanol concentrations above the optimal one (Figure 4, S15).



Scheme 1. A visual representation of the reactions assumed to occur in the model. Lithium metal is plated from lithium ions in solution by the application of a current, yielding solid lithium. The lithium metal can react with the proton carrier (HA) to form hydrogen, or with nitrogen to form lithium nitride. Lithium nitride is protonated quickly to form ammonia and does not contribute to measured kinetics; this reaction is kinetically facile and is not probed by our kinetic analyses.

As the experiments were performed galvanostatically, we introduce an applied current density I into the model. We have experimentally observed that almost all the current applied goes towards lithium plating; only a small fraction of the current, typically ~1%, goes towards other reactions (Figure S13, S14), likely EtOH or water reduction. For simplicity, we assume all the current goes towards lithium plating in the model. The lithium can then react only via one of the

two aforementioned reactions (Scheme 1); we assume no other side reactions, such as SEI formation, occur. The rate of change of lithium concentration is given by:

$$F \frac{d[Li]}{dt} = I - k_1[Li]^\alpha [EtOH]^x - k_2[Li]^\beta [N_2] \quad (4)$$

From the QSSA assumption made for lithium and the relative rates of ammonia and hydrogen evolution (Eq. 3), the lithium concentration can be solved for in terms of applied current density:

$$I - k_1[Li]^\alpha [EtOH]^x - k_2[Li]^\beta [N_2] \approx I - k_1[Li]^\alpha [EtOH]^x \approx 0 \quad (5)$$

$$[Li] = \left(\frac{1}{k_1 [EtOH]^x} \right)^{\frac{1}{\alpha}} I^{\frac{1}{\alpha}} \quad (6)$$

The FE for ammonia can be found to be:

$$FE_{NH_3} = \frac{k_2[Li]^\beta [N_2]}{I} \approx \frac{k_2[Li]^\beta [N_2]}{k_1[Li]^\alpha [EtOH]^x} = \left(\frac{k_2}{k_1^{1+\frac{\beta-\alpha}{\alpha}}} \right) \frac{[N_2]}{[EtOH]^{x(1+\frac{\beta-\alpha}{\alpha})}} I^{\frac{\beta-\alpha}{\alpha}} \quad (7)$$

According to this model, named the kinetic-only model, the ammonia FE should change with current density as $I^{\frac{\beta-\alpha}{\alpha}}$. Experimental data (Figure 5) suggest that $\frac{\beta-\alpha}{\alpha} = \frac{1}{2}$. One possible interpretation of this result is that $\alpha = 2$ and $\beta = 3$, which corresponds to the number of lithium atoms required to produce one molecule of H₂ or NH₃, respectively.

The model predicts that the ammonia FE should decrease with increasing ethanol concentration, with an order equal to $-x \left(1 + \frac{\beta-\alpha}{\alpha} \right) = -x \left(1 + \frac{1}{2} \right)$. As the observed order for ethanol from experimental data is -1.5, we can deduce that $x = 1$, from which we infer that the reaction between lithium and ethanol is first order in ethanol. The observed non-integer order for

ammonia FE as a function of ethanol concentration is thus explained by a combination of increased competition from ethanol and decreased availability of lithium to form ammonia.

The FE towards ammonia exhibits a peak as applied current density is varied, which is unexplained by the kinetic model. One explanation for the FE peaking behavior could be a change in the morphology in the plated lithium at higher current densities, and thus a change in its reactivity. Lithium morphology has been observed to change at higher current densities, often turning more dendritic.³⁴ However, if changes in morphology led to changes in reactivity, the production rate of ammonia could be expected to decrease alongside the FE, which is not observed (Figure 5C).

Alternatively, the lithium concentration could be reaching a maximum possible value at high current densities; this may be reflected in the analytical model as a constant, maximum value of $[Li]$. One of the assumptions made in the model is that the rates of reactions are proportional to the amount of lithium on the surface. This assumption breaks down when lithium is plated rapidly enough to begin plating on top of itself. This could result in a fraction of lithium that cannot contribute to ammonia or hydrogen formation. Visually, there is not a clear difference in the amount of lithium plated at different current densities after electrolysis (Figure S7). However, this does not necessarily disprove this hypothesis, as the difference between thinner and thicker lithium layers may be difficult to observe by visual inspection. In order to reject this hypothesis, we performed an experiment where the concentration of ethanol was decreased to 0.1 M while maintaining the applied current density of 15 mA cm^{-2} , thus increasing the amount of lithium present (Eq. 6). If the lithium concentration was reaching a finite maximum value, then the FE for ammonia would be unaffected. This was not observed; the FE increased to $15.2 \pm 3.1\%$ (Figure

6), which is higher than the previously observed value of $8.6 \pm 2.2\%$. Thus, a maximum lithium concentration is not the cause of a peak in ammonia FE.

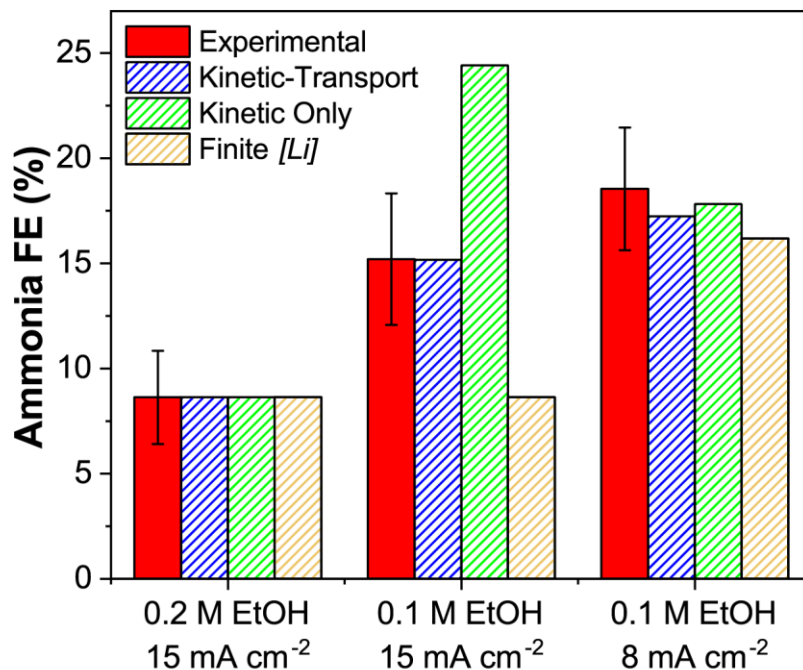


Figure 6. A comparison between proposed kinetic models. The models seek to explain the appearance of an optimum current density to maximize FE. The expressions for the finite lithium concentration model described in the text are given in the Supporting Information. All models use the 0.2 M EtOH, 15 mA cm⁻² point to fit parameters. Only the coupled kinetic-transport model matches experimental results well under all conditions. Error bars represent the standard deviation between replicates of the same experiment with $n = 3$.

Another way to explain the observed optimal current density is that the peak is caused by a local decrease of dissolved nitrogen concentration at the electrode surface due to the limited rate of diffusion of nitrogen. In this case, the partial current density for ammonia would be approaching the mass transfer limited current density.³⁵ While the limiting current (see SI) is significantly higher than the peak partial current towards ammonia (11 ± 8 mA cm⁻² versus 1.3 ± 0.3 mA cm⁻²), transport limitations can still be used to explain the peak behavior, as shown by modifying the model below. The rate of diffusion of nitrogen in units of current density to the electrode surface is given by:³⁵

$$N_{N_2} = \frac{6FD}{\delta} (C_{bulk} - [N_2]) \quad (8)$$

Nitrogen diffusing to the surface will react with lithium according to Eq. 2. Over time, the system will reach a steady state, in which the concentration profile of nitrogen in the transport boundary layer does not change with time. At this point, the reaction rate of the nitrogen will be equal to its diffusion rate:

$$\frac{6FD}{\delta} (C_{bulk} - [N_2]) = k_2 [Li]^\beta [N_2] \quad (9)$$

Solving for the concentration of nitrogen at the surface, we obtain:

$$[N_2] = \frac{C_{bulk}}{1 + \frac{\delta}{6FD} k_2 [Li]^\beta} \quad (10)$$

At this point, we can derive an expression for the FE towards ammonia. We once again assume the partial current for hydrogen is significantly higher than the partial current for ammonia (Eq. 3). The same conclusions are obtained regardless of whether this assumption is made; we make it in order to simplify the resulting expressions. The Faradaic efficiency towards ammonia is given by:

$$FE_{NH_3} = \frac{k_2 [Li]^\beta [N_2]}{k_2 [Li]^\beta [N_2] + k_1 [Li]^\alpha [EtOH]^x} \approx \frac{[Li]^{\beta-\alpha} [N_2]}{\left(\frac{k_1}{k_2} [EtOH]^x\right)} = \frac{C_{bulk} [Li]^{\beta-\alpha}}{\left(\frac{k_1}{k_2} [EtOH]^x\right) \left(1 + \frac{\delta}{6FD} k_2 [Li]^\beta\right)} \quad (11)$$

Substituting the expression for lithium concentration (Eq. 6), we obtain:

$$FE_{NH_3} = \frac{C_{bulk} l^{\frac{\beta-\alpha}{\alpha}}}{\left(\frac{\beta}{k_2} \frac{k_1}{k_2} [EtOH]^x \left(1 + \frac{\beta-\alpha}{\alpha}\right)\right) \left(1 + \frac{\delta k_2}{6FD k_1^\alpha} \frac{\beta}{l^\alpha} \frac{\beta}{[EtOH]^\alpha} \frac{\beta^x}{\alpha^x}\right)} \quad (12)$$

This model is named the kinetic-transport model. It can be shown that when ammonia FE is maximized by varying the applied current density, the partial current density towards ammonia is one third of the transport limited current density (see Figure S8, Supplemental Information):

$$I_{peak} = \frac{I_{lim}}{3} \quad (13)$$

From this result, we can conclude that the FE towards ammonia can exhibit a peak with respect to applied current density at any fixed ethanol concentration due to transport limitations with a partial current that is only a third of the predicted transport limited current. The partial current towards ammonia at peak FE is $1.3 \pm 0.3 \text{ mA cm}^{-2}$ (Figure 5), which implies that the limiting current density in the system is $3.9 \pm 0.9 \text{ mA cm}^{-2}$. This value lies within the estimated range of possible limiting current densities ($11 \pm 8 \text{ mA cm}^{-2}$, see SI); hence, it is possible that some transport effects are observed at higher current densities.

The above model predicts that decreasing the ethanol concentration from 0.2 M to 0.1 M while applying 15 mA cm^{-2} increases both the production rate and FE towards ammonia, which was experimentally observed (Figure 6). According to the model, if transport limitations are present, the obtained value of FE is not optimal, as the partial current density towards ammonia is above one third of the transport limited current, which was measured at 0.2 M ethanol ($2.3 \pm 0.5 \text{ mA cm}^{-2}$ vs $1.3 \pm 0.3 \text{ mA cm}^{-2}$). Therefore, decreasing the applied current density should increase the Faradaic efficiency. This is, in fact, observed; at 8 mA cm^{-2} and 0.1 M, the Faradaic efficiency increases to $18.5 \pm 2.9\%$ (Figure 6), which further supports the hypothesis that nitrogen transport limitations are observed in this system. As lowering the concentration of ethanol further would decrease ammonia production (Figure 4), this FE is close to optimal in this system. Under these conditions, ammonia is produced at an energy efficiency of 1.45%, with most of the energy lost to

resistive dissipation (Figure S16). While we did not explicitly optimize for energy efficiency, it is an important metric to consider when designing electrochemical nitrogen reduction systems.

Conclusion

In summary, this work demonstrates that lithium metal chemistry can be used to fix nitrogen to ammonia continuously in a non-aqueous solvent at high rates at room temperature and ambient pressure. We found that the reaction between nitrogen and lithium is promoted by a small amount of proton carrier, in this case ethanol. We measured rate laws for the reactions between lithium, ethanol, and nitrogen by varying the applied current density and concentrations of relevant species. We found that the lithium nitridation and lithium protonation reactions are first order in nitrogen and ethanol, respectively. The orders with respect to lithium differ for the two reactions, with the nitridation reaction being more sensitive to the amount of lithium present. Due to this difference, the FE towards ammonia was found to increase with increasing applied current density. This finding could potentially allow for development of a process that can produce ammonia at higher FEs. In the present system, the FE for ammonia reaches a maximum value when varying current density while maintaining a high production rate, likely due to nitrogen transport limitations. We hope that mechanistic understanding of this system will serve as a starting point and inspiration for the development of more efficient continuous lithium-mediated methods to produce ammonia.

Experimental Procedures

A polished copper foil served as the cathode, onto which lithium was plated electrochemically; a platinum foil served as the anode; and a polyporous polyethylene separator (Daramic 175) was used to separate the chambers of a PEEK electrochemical cell (Figure S1, S2.

The use of a separator prevented bulk convection of ammonia from the cathode to the anode, at which ammonia may be oxidized (Figure S11). The electrolyte solution consisted of 1 M lithium tetrafluoroborate (LiBF_4) dissolved in molecular sieve-dried tetrahydrofuran (THF) with varying concentrations of ethanol (EtOH). A detailed description of the cell geometry, electrolyte preparation procedure, and other experimental details can be found in the Supporting Information. The choice of solvent and proton carrier was based on previous work,¹⁵ while the electrolyte and lithium source were chosen for safety and economic reasons. Many factors are essential to obtain high ammonia yields, including dryness of the solvent (Figure S9), purity of the reagents (Figure S10), and the use of a thick separator (Figure S11).

The cathode compartment of the cell was continuously purged with 10 sccm of THF-saturated N_2 gas both before polarization and during the experiment. Lithium metal was galvanostatically plated onto the copper cathode. The lithium metal reacted continuously with nitrogen dissolved in the electrolyte solution to form lithium nitride, which was subsequently protonated by the ethanol in solution to form ammonia (Figure 1A). The electrolyte solution containing ammonia was diluted with water; the ammonia content of the resulting solution was quantified using the salicylate method.^{16,36,37}

Acknowledgements

Funding for this research was provided by the Abdul Latif Jameel World Water and Food Systems Lab (J-WAFS) at MIT. This material is based upon work supported by the National Science Foundation Graduate Research Fellowship under Grant No. 1122374. We thank Matt Wolski of Daramic for providing us with polyporous separator samples. We thank Yuzhang Li and Nathan Corbin for productive and helpful discussions.

Author Contributions

Conceptualization, N.L. and K.M.; Methodology, N.L.; Investigation, N.L.; Validation, Z.J.S.; Writing – Original Draft, N.L.; Writing – Review & Editing – N.L., K.W., and K.M.; Supervision. K.M.

Declaration of Interests

The authors declare no competing interests.

References

- [1] Food and Agriculture Organization of United Nations. World fertilizer trends and outlook to 2020. Rome: 2017.
- [2] Erisman JW, Sutton MA, Galloway J, Klimont Z, Winiwarter W. How a century of ammonia synthesis changed the world. *Nat Geosci* 2008;1:636–9. doi:10.1038/ngeo325.
- [3] Giddey S, Badwal SPS, Munnings C, Dolan M. Ammonia as a Renewable Energy Transportation Media. *ACS Sustain Chem Eng* 2017;5:10231–9. doi:10.1021/acssuschemeng.7b02219.
- [4] Nørskov J, Chen J. Sustainable Ammonia Synthesis: Exploring the scientific challenges associated with discovering alternative, sustainable processes for ammonia production. Dulles, VA: 2016.
- [5] Kahrl F, Li Y, Su Y, Tennigkeit T, Wilkes A, Xu J. Greenhouse gas emissions from nitrogen fertilizer use in China. *Environ Sci Policy* 2010;13:688–94. doi:10.1016/j.envsci.2010.07.006.
- [6] Institute for Industrial Productivity. Ammonia. *Ind Effic Technol Database* n.d. <http://ietd.iipnetwork.org/content/ammonia> (accessed August 14, 2018).
- [7] Foster SL, Bakovic SIP, Duda RD, Maheshwari S, Milton RD, Minteer SD, et al. Catalysts for nitrogen reduction to ammonia. *Nat Catal* 2018;1:490–500. doi:10.1038/s41929-018-0092-7.
- [8] Schiffer ZJ, Manthiram K. Electrification and Decarbonization of the Chemical Industry. *Joule* 2017;1:10–4. doi:10.1016/j.joule.2017.07.008.
- [9] Chen JG, Crooks RM, Seefeldt LC, Bren KL, Bullock RM, Darensbourg MY, et al. Beyond fossil fuel–driven nitrogen transformations. *Science* 2018;360:eaar6611. doi:10.1126/science.aar6611.
- [10] Bao D, Zhang Q, Meng F-L, Zhong H-X, Shi M-M, Zhang Y, et al. Electrochemical

- Reduction of N₂ under Ambient Conditions for Artificial N₂ Fixation and Renewable Energy Storage Using N₂/NH₃ Cycle. *Adv Mater* 2017;29:1604799. doi:10.1002/adma.201604799.
- [11] Kong J, Lim A, Yoon C, Jang JH, Ham HC, Han J, et al. Electrochemical Synthesis of NH₃ at Low Temperature and Atmospheric Pressure Using a γ -Fe₂O₃ Catalyst. *ACS Sustain Chem Eng* 2017;5:10986–95. doi:10.1021/acssuschemeng.7b02890.
- [12] Yang X, Nash J, Anibal J, Dunwell M, Kattel S, Stavitski E, et al. Mechanistic Insights into Electrochemical Nitrogen Reduction Reaction on Vanadium Nitride Nanoparticles. *J Am Chem Soc* 2018;140:13387–91. doi:10.1021/jacs.8b08379.
- [13] Furuya N, Yoshida H. Electroreduction of nitrogen to ammonia on gas-diffusion electrodes loaded with inorganic catalyst. *J Electroanal Chem* 1990;291:269–72.
- [14] Lv C, Qian Y, Yan C, Ding Y, Liu Y, Chen G, et al. Defect Engineering Metal-Free Polymeric Carbon Nitride Electrocatalyst for Effective Nitrogen Fixation under Ambient Conditions. *Angew Chemie Int Ed* 2018;57:10246–50. doi:10.1002/anie.201806386.
- [15] Tsuneto A, Kudo A, Sakata T. Lithium-mediated electrochemical reduction of high pressure N₂ to NH₃. *J Electroanal Chem* 1994;367:183–8. doi:10.1016/0022-0728(93)03025-K.
- [16] McEnaney JM, Singh AR, Schwalbe JA, Kibsgaard J, Lin JC, Cargnello M, et al. Ammonia synthesis from N₂ and H₂O using a lithium cycling electrification strategy at atmospheric pressure. *Energy Environ Sci* 2017;10:1621–30. doi:10.1039/C7EE01126A.
- [17] Ma J-L, Bao D, Shi M-M, Yan J-M, Zhang X-B. Reversible Nitrogen Fixation Based on a Rechargeable Lithium-Nitrogen Battery for Energy Storage. *Chem* 2017;2:525–32. doi:10.1016/j.chempr.2017.03.016.
- [18] Kim K, Lee SJ, Kim D-Y, Yoo C-Y, Choi JW, Kim J-N, et al. Electrochemical Synthesis of Ammonia from Water and Nitrogen: A Lithium-Mediated Approach Using Lithium-Ion Conducting Glass Ceramics. *ChemSusChem* 2018;11:120–4. doi:10.1002/cssc.201701975.
- [19] Cui X, Tang C, Zhang Q. A Review of Electrocatalytic Reduction of Dinitrogen to Ammonia under Ambient Conditions. *Adv Energy Mater* 2018;8:1800369. doi:10.1002/aenm.201800369.
- [20] Kyriakou V, Garagounis I, Vasileiou E, Vourros A, Stoukides M. Progress in the Electrochemical Synthesis of Ammonia. *Catal Today* 2017;286:2–13. doi:10.1016/j.cattod.2016.06.014.
- [21] Greenwood NN., Earnshaw A. *Chemistry of the Elements*. 2nd Editio. Elsevier; 1997.
- [22] Greenlee LF, Renner JN, Foster SL. The Use of Controls for Consistent and Accurate Measurements of Electrocatalytic Ammonia Synthesis from Dinitrogen. *ACS Catal* 2018;8:7820–7. doi:10.1021/acscatal.8b02120.
- [23] Zhang L, Ji X, Ren X, Luo Y, Shi X, Asiri AM, et al. Efficient Electrochemical N₂ Reduction to NH₃ on MoN Nanosheets Array under Ambient Conditions. *ACS Sustain*

- Chem Eng 2018;acssuschemeng.8b01438. doi:10.1021/acssuschemeng.8b01438.
- [24] Zhang R, Zhang Y, Ren X, Cui G, Asiri AM, Zheng B, et al. High-Efficiency Electrosynthesis of Ammonia with High Selectivity under Ambient Conditions Enabled by VN Nanosheet Array. *ACS Sustain Chem Eng* 2018;6:9545–9. doi:10.1021/acssuschemeng.8b01261.
- [25] Chen G-F, Cao X, Wu S, Zeng X, Ding L-X, Zhu M, et al. Ammonia Electrosynthesis with High Selectivity under Ambient Conditions via a Li⁺ Incorporation Strategy. *J Am Chem Soc* 2017;139:9771–4. doi:10.1021/jacs.7b04393.
- [26] Zhou F, Azofra LM, Ali M, Kar M, Simonov AN, McDonnell-Worth C, et al. Electro-synthesis of ammonia from nitrogen at ambient temperature and pressure in ionic liquids. *Energy Environ Sci* 2017;10:2516–20. doi:10.1039/C7EE02716H.
- [27] Berger S, Braun S, Kalinowski H-O. *NMR Spectroscopy of the Non-Metallic Elements*. 2nd Editio. Bonn: John Wiley & Sons, Inc; 1988.
- [28] Dabundo R, Lehmann MF, Treibergs L, Tobias CR, Altabet MA, Moisander PH, et al. The Contamination of Commercial ¹⁵N₂ Gas Stocks with ¹⁵N-Labeled Nitrate and Ammonium and Consequences for Nitrogen Fixation Measurements. *PLoS One* 2014;9:e110335. doi:10.1371/journal.pone.0110335.
- [29] Minteer SD, Christopher P, Linic S. Recent Developments in Nitrogen Reduction Catalysts: A Virtual Issue. *ACS Energy Lett* 2018;163–6. doi:10.1021/acsenerylett.8b02197.
- [30] Wang H, Zhang W-D, Deng Z-Q, Chen M-C. Interaction of nitrogen with lithium in lithium ion batteries. *Solid State Ionics* 2009;180:212–5. doi:10.1016/j.ssi.2008.12.001.
- [31] Peled E, Menkin S. Review—SEI: Past, Present and Future. *J Electrochem Soc* 2017;164:A1703–19. doi:10.1149/2.1441707jes.
- [32] McFarlane EF, Tompkins FC. Nitridation of lithium. *Trans Faraday Soc* 1962;58:997. doi:10.1039/tf9625800997.
- [33] Atkins P. *Physical Chemistry*. 6th Editio. New York: W.H. Freeman and Company; 1998.
- [34] An SJ, Li J, Daniel C, Mohanty D, Nagpure S, Wood DL. The state of understanding of the lithium-ion-battery graphite solid electrolyte interphase (SEI) and its relationship to formation cycling. *Carbon N Y* 2016;105:52–76. doi:10.1016/j.carbon.2016.04.008.
- [35] Bard AJ, Faulkner LR. *Electrochemical Methods. Fundamentals and Applications*. 2nd Editio. Phoenix: John Wiley & Sons, Inc; 2001.
- [36] Verdouw H, Van Echteld CJA, Dekkers EMJ. Ammonia determination based on indophenol formation with sodium salicylate. *Water Res* 1978;12:399–402. doi:10.1016/0043-1354(78)90107-0.
- [37] Yu X, Han P, Wei Z, Huang L, Gu Z, Peng S, et al. Boron-Doped Graphene for Electrocatalytic N₂ Reduction. *Joule* 2018;2:1–13. doi:10.1016/j.joule.2018.06.007.

Supplemental Figures and Tables

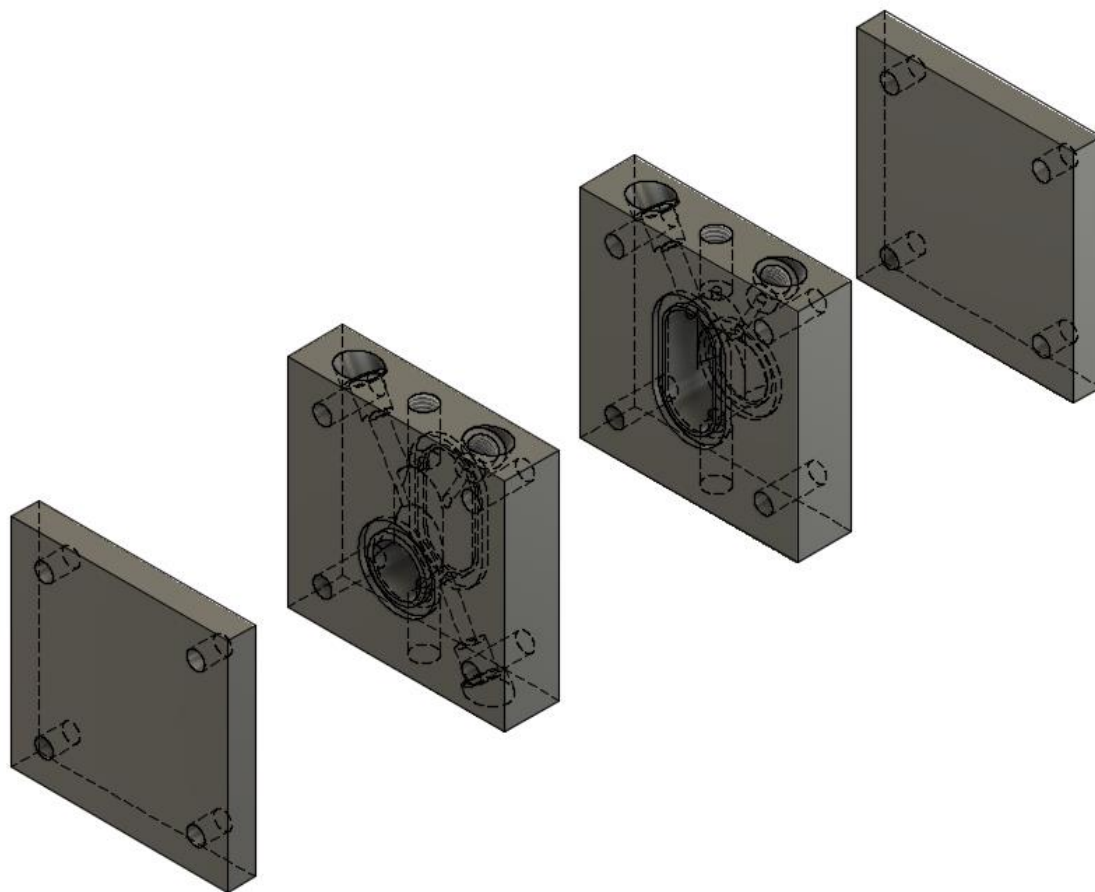


Figure S1. A CAD drawing of the PEEK electrochemical cell used in all experiments. O-rings are used to seal the cell on both sides of the anode and cathode compartments and are not depicted. ETFE 1/4-28 plastic fittings were used at the inlet and outlet ports with 1/8" FEP tubing to transfer the feed gas. The cell design is similar to one previously reported in the literature.¹ The cell was manufactured by Lab Machinist Solutions.

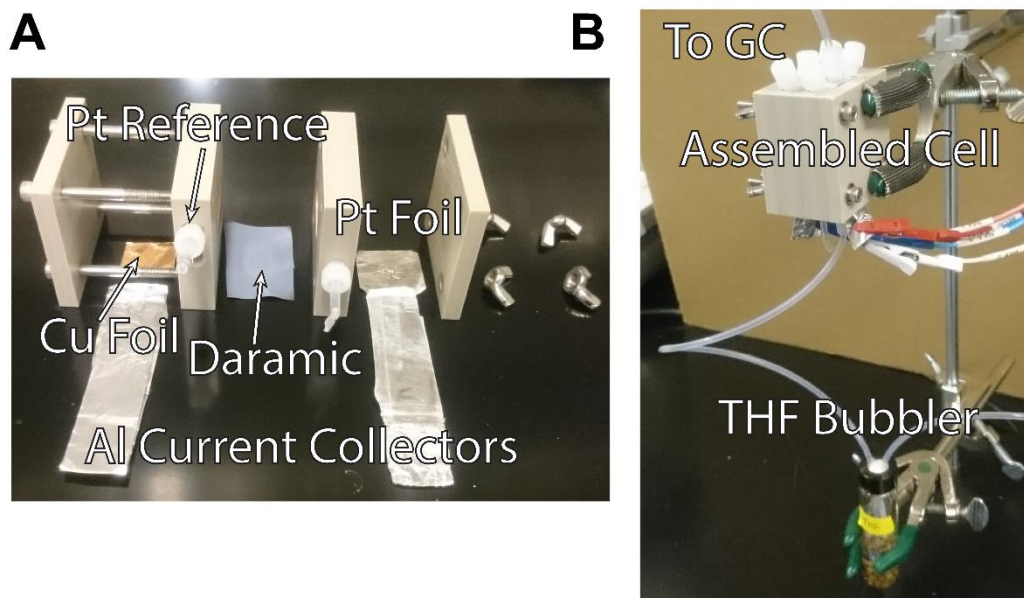


Figure S2. Photographs of (A) the disassembled cell and of (B) the setup used to run experiments. Nitrogen is fed via an Alicat flow controller to a bubbler filled with THF to saturate the gas, after which it enters the cell. The bubbler is made by sealing a glass vial with a rubber septum and inserting two 1/8" FEP tubes to have gas come in and out of the bubbler. Dried molecular sieves are added to the THF to maintain dryness of inlet gas and electrolyte in the cell. The gas flowing out of the cathode can be sent to a GC for hydrogen quantification.

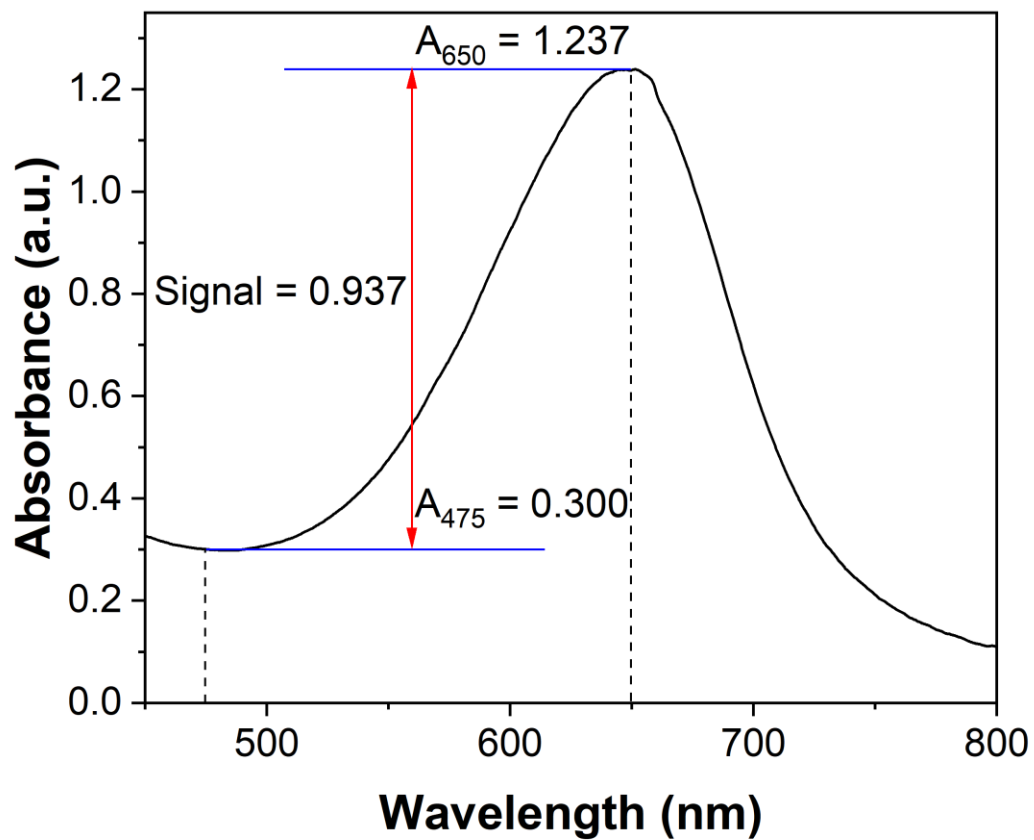


Figure S3. The absorbance signal used to quantify ammonia. The signal is taken to be the difference between the absorbance at 650 nm and 475 nm.

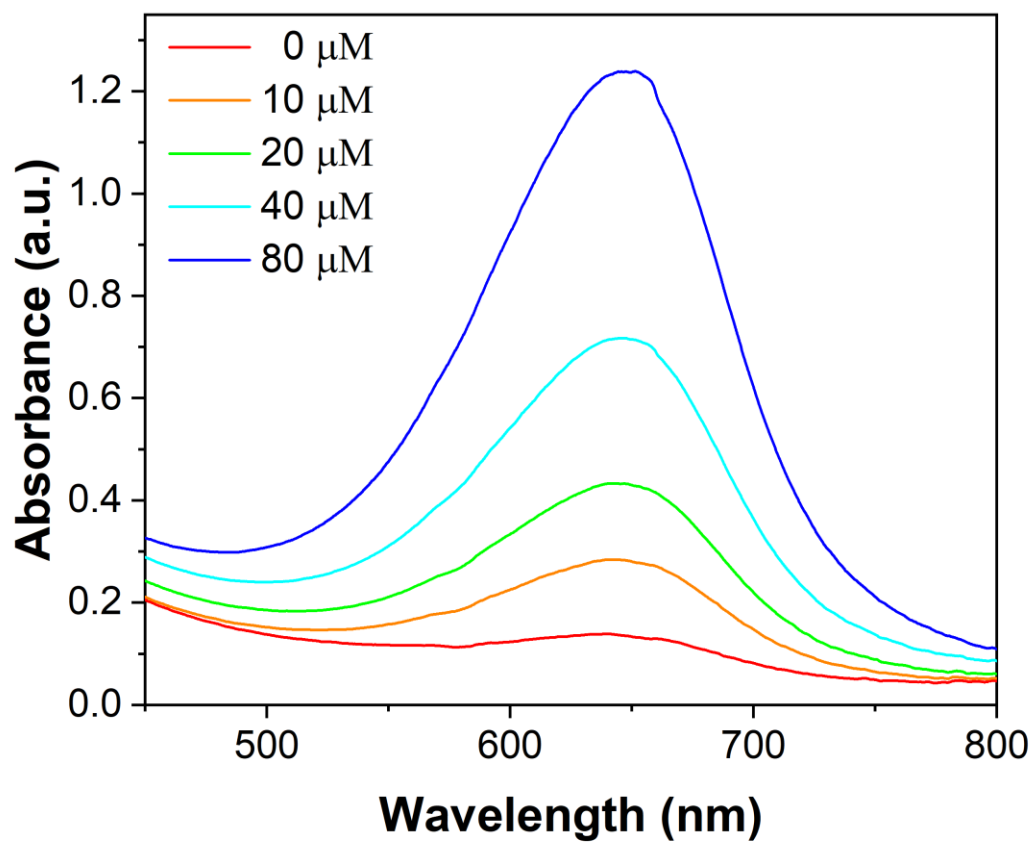


Figure S4. Absorbance spectra of calibration solutions containing 10% of LiBF₄/EtOH/THF electrolyte solution used in experiments, 90% water in addition to the specified ammonia concentration.

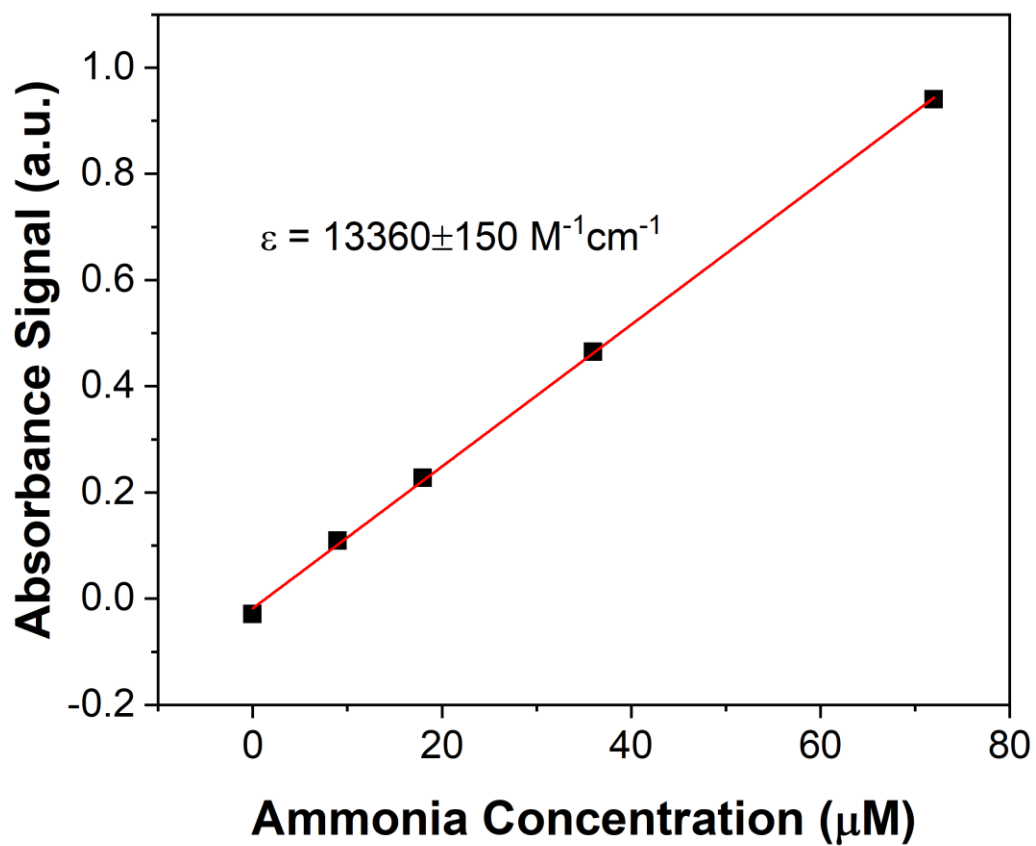


Figure S5. A typical calibration curve obtained for samples containing 10% of LiBF₄/THF electrolyte solution in addition to the specified ammonia concentration.

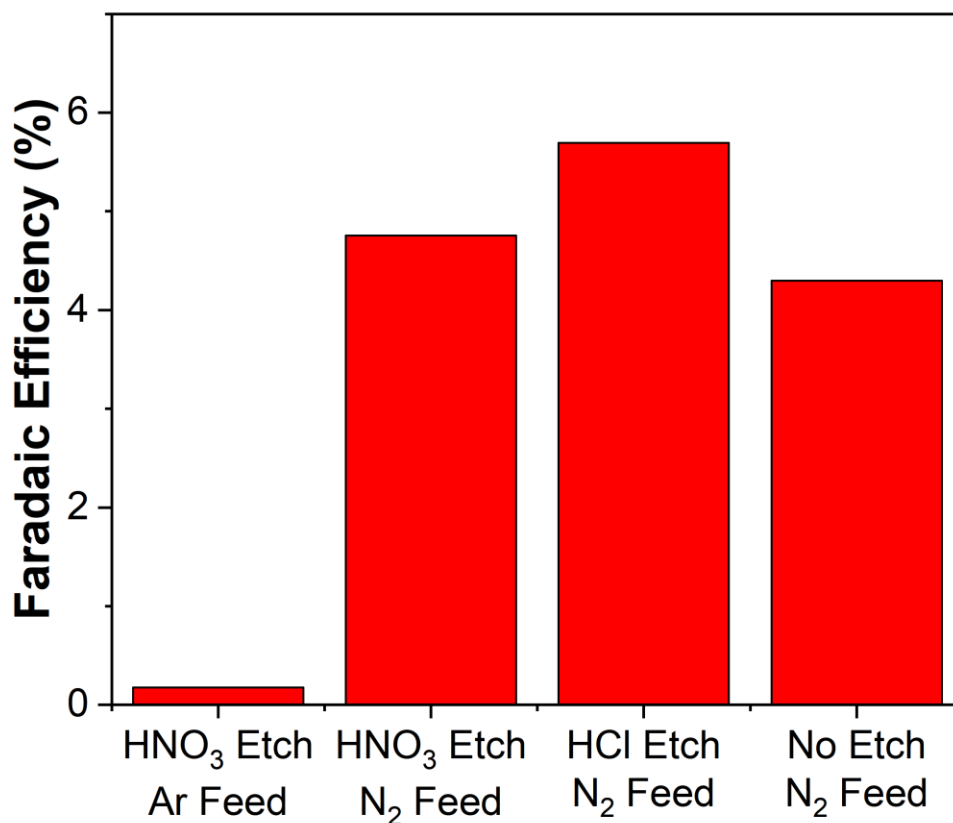


Figure S6. Results of control experiments aimed to eliminate the possibility of ammonia contamination from HNO₃ etching (see Supplemental Experimental Procedures – Cathode Preparation). Copper foils at the cathode were polished with sandpaper and treated with HNO₃, HCl, or not treated with acid. N₂ and Ar were used as feed gases in electrochemical experiments. The lack of ammonia detected with Ar as the feed gas with a HNO₃-treated foil and the presence of ammonia in HCl-treated and untreated foils with N₂ as the feed gas confirms that HNO₃ contamination is not responsible for ammonia formation.

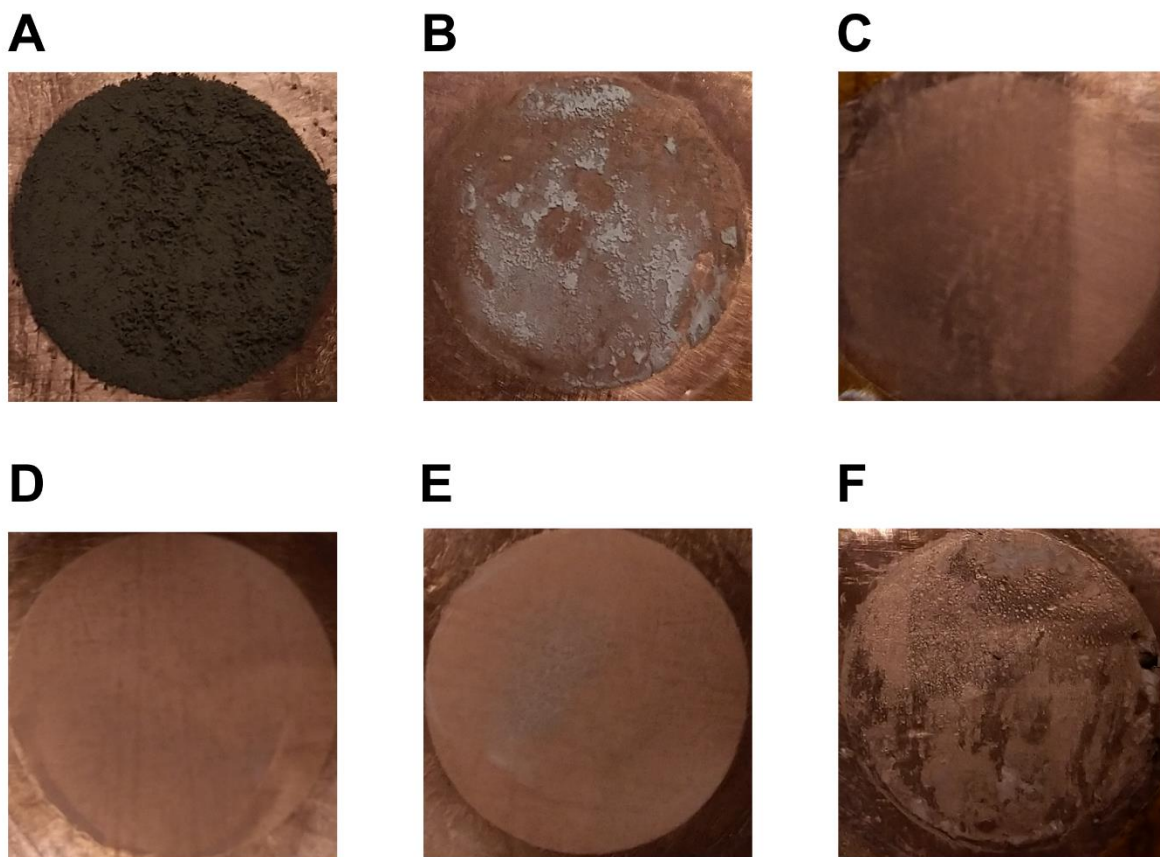


Figure S7. Images of the amount of solids remaining on the cathode after electrolysis with different (A-C) ethanol concentrations and (D-F) applied current density. The exact conditions used were: (A) 3 mA cm^{-2} , 0.025 M EtOH , (B) 3 mA cm^{-2} , 0.1 M EtOH , (C) 3 mA cm^{-2} , 0.4 M EtOH (D) 3 mA cm^{-2} , 0.2 M EtOH , (E) 15 mA cm^{-2} , 0.2 M EtOH , (F) 25 mA cm^{-2} , 0.2 M EtOH . The amount of solids decreases with increasing ethanol concentration. It does not seem to change with increasing current density.

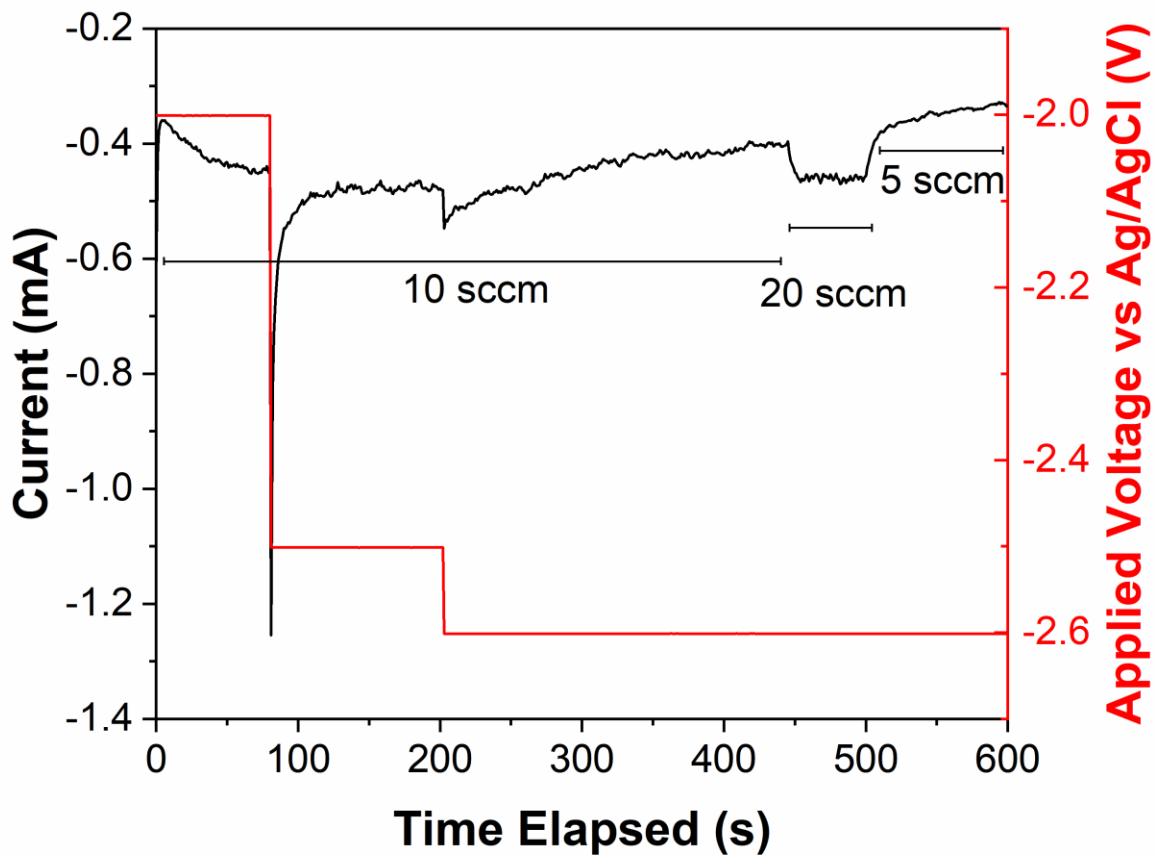


Figure S8. Ferrocenium limiting current density experiment data. Note the changing bubbling rate throughout the experiment. The current density does not change with potential, which means that the limiting current has been achieved. $0.45 \pm 0.05 \text{ mA cm}^{-2}$ was the value assumed for a 10 sccm bubbling rate.

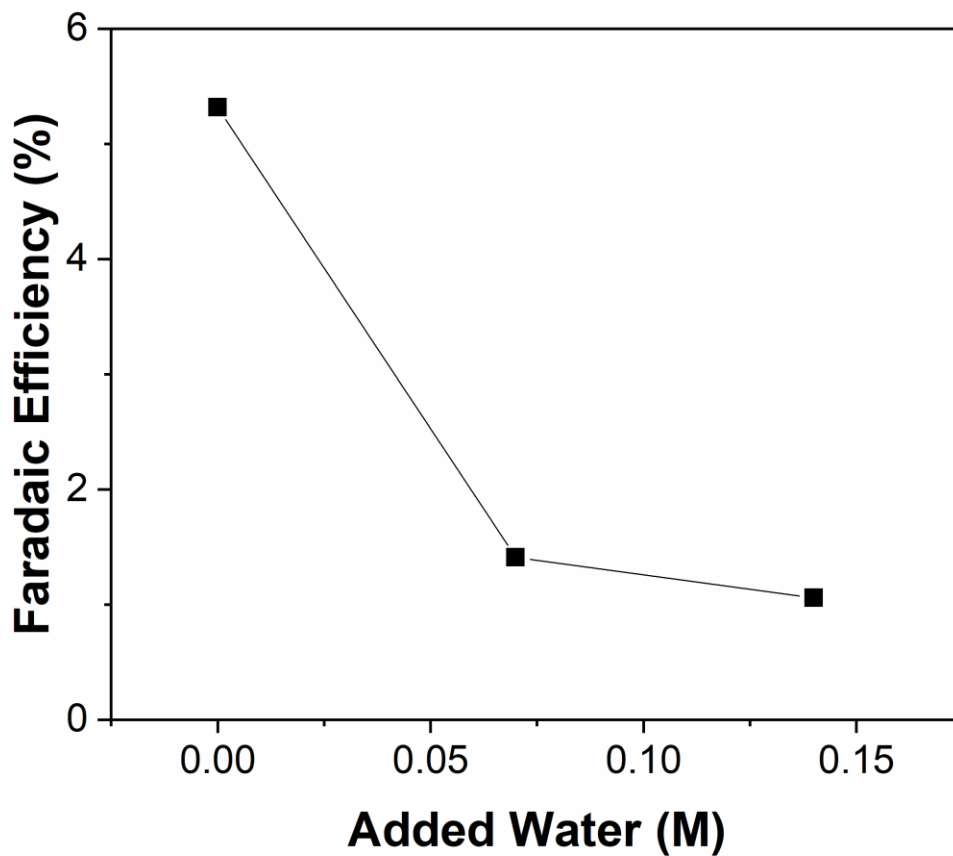


Figure S9. The effect of addition of water to a 0.2 M EtOH, 1M LiBF₄, THF electrolyte solution in a 3 mA cm⁻² experiment. The presence of water in the solution was found to significantly impact the Faradaic efficiency towards ammonia. Both the LiBF₄ salt and THF solvent must be dry. 1% of water by mass in the LiBF₄ corresponds to an increase in water concentration by 0.05 M. The content of water in the as-purchased THF was found to be approximately 0.03 M.

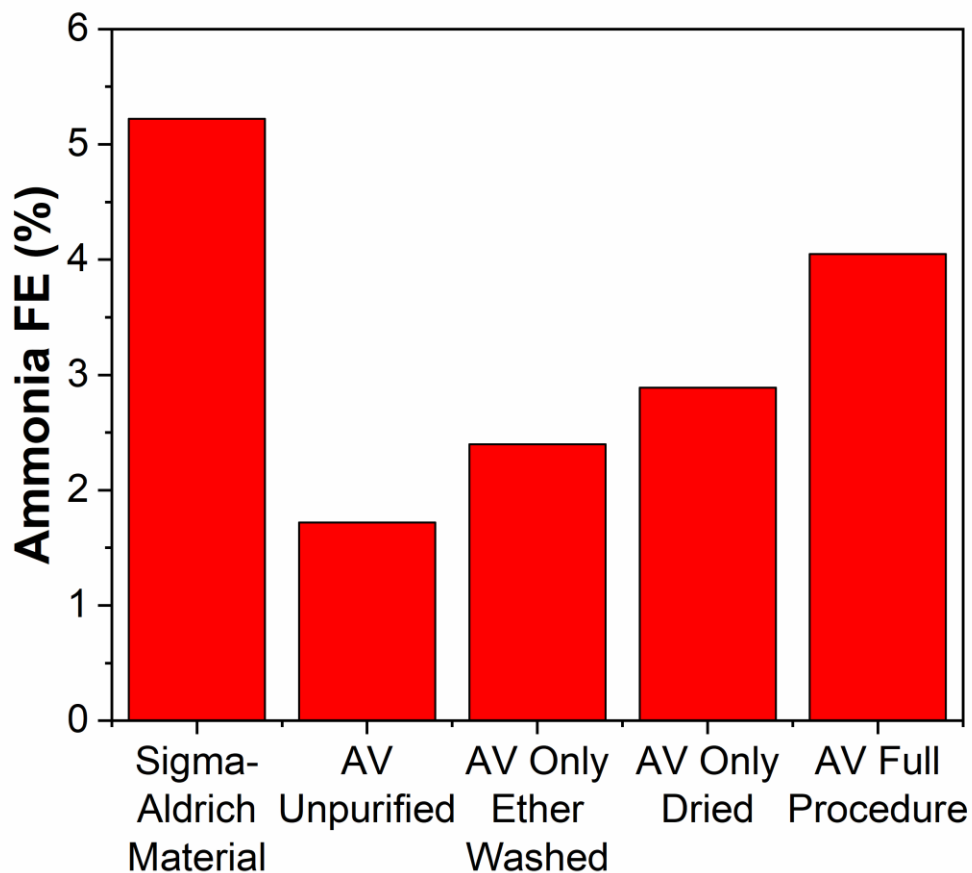


Figure S10. Comparison of ammonia yields when using LiBF₄ of various purities. LiBF₄ from Sigma-Aldrich, used throughout this work, leads to high ammonia FE. LiBF₄ from alternative vendors (AV), including Alfa Aesar, TCI America, and BeanTown Chemical, does not give good results when used as received. Simply washing it with diethyl ether or drying at 110°C increases the ammonia yields somewhat. Using the full purification procedure described in Supplemental Experimental Procedures improves yields significantly by removing impurities and water from the electrolyte. The yield is still ~20% lower than when using Sigma-Aldrich LiBF₄, however.

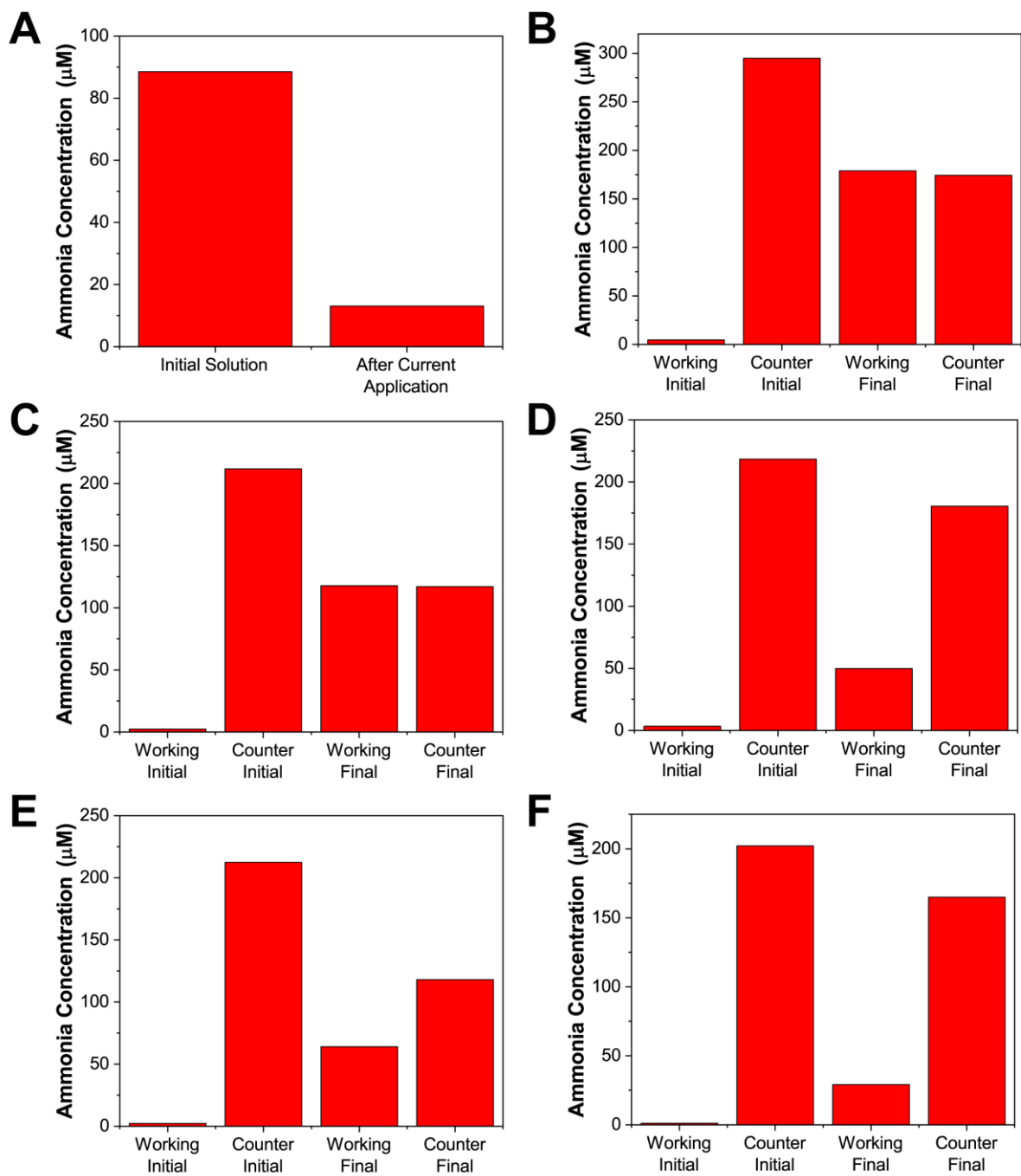


Figure S11. Oxidation of ammonia at the anode and diffusion of ammonia through the separator. (A) A decrease in the concentration of ammonia in an electrolyte after application of potential due to oxidation at the anode. Equilibration of two cell chambers separated by a PTFE filter membrane after (B) 15 hours, (C) 2 hours, and (D) 20 minutes. Approach to equilibrium of two cell chambers separated by Daramic 175 after (E) 3 hours and (F) 40 minutes.

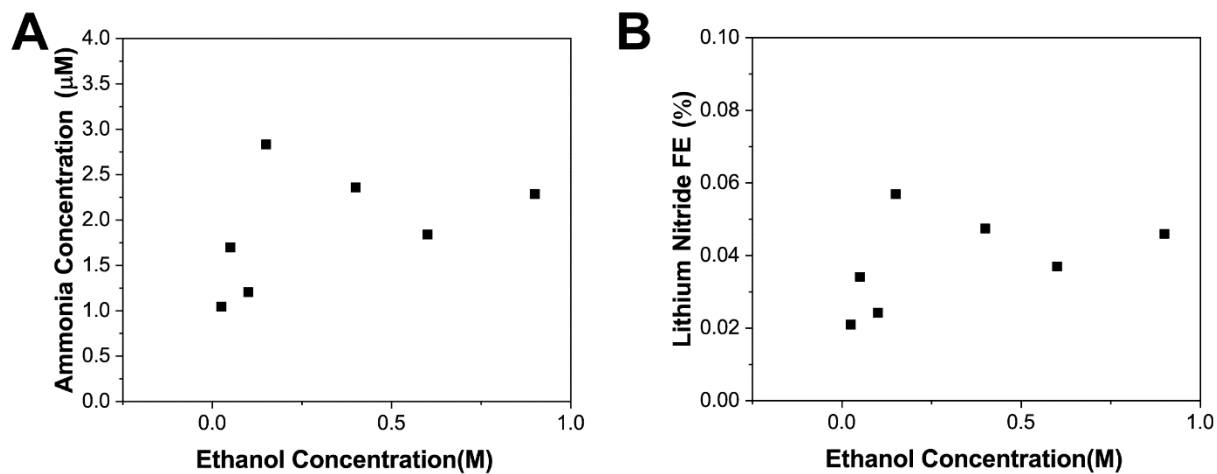


Figure S12. (A) The concentration of ammonia measured in solution made after dissolving solid residue left on the copper cathode after electrolysis in 0.1 M HCl and (B) the corresponding lithium nitride FE as a function of ethanol concentration. There is not an appreciable amount of ammonia detected, even at low ethanol concentrations, where significant amounts of solid residue remain on the cathode. This means that the residue is predominantly unreacted lithium, and any nitride formed during the experiment is quickly protonated by ethanol to form ammonia and does not accumulate over time.

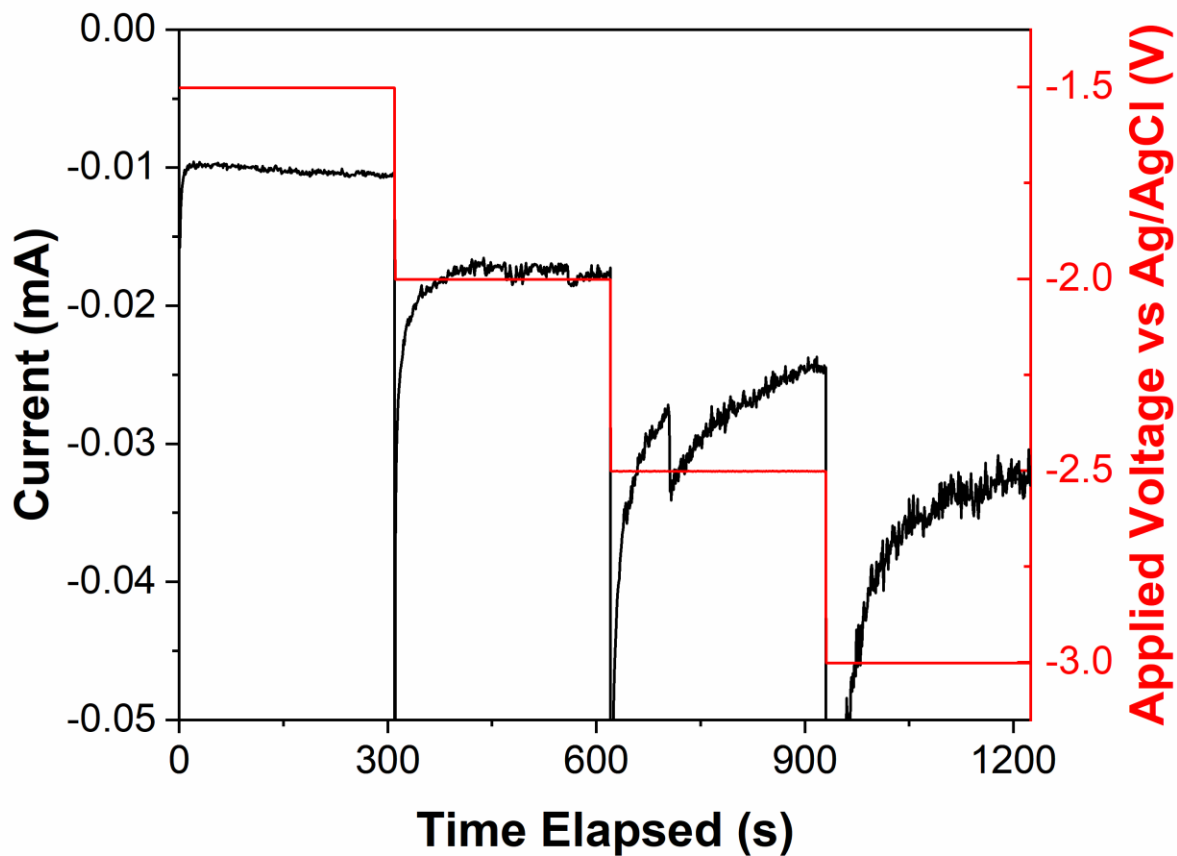


Figure S13. Measured currents in a cell with 1 M LiBF₄, 0.2 M EtOH solution in THF with N₂ bubbling at potentials less negative than required to plate lithium. These currents would most likely come from electrochemical reactions other than lithium plating, such as residual water or ethanol reduction to produce H₂. While the currents at these potentials are non-zero, they are significantly below the currents used in our galvanostatic experiments. This means we can assume that almost all the current goes towards lithium plating when developing models.

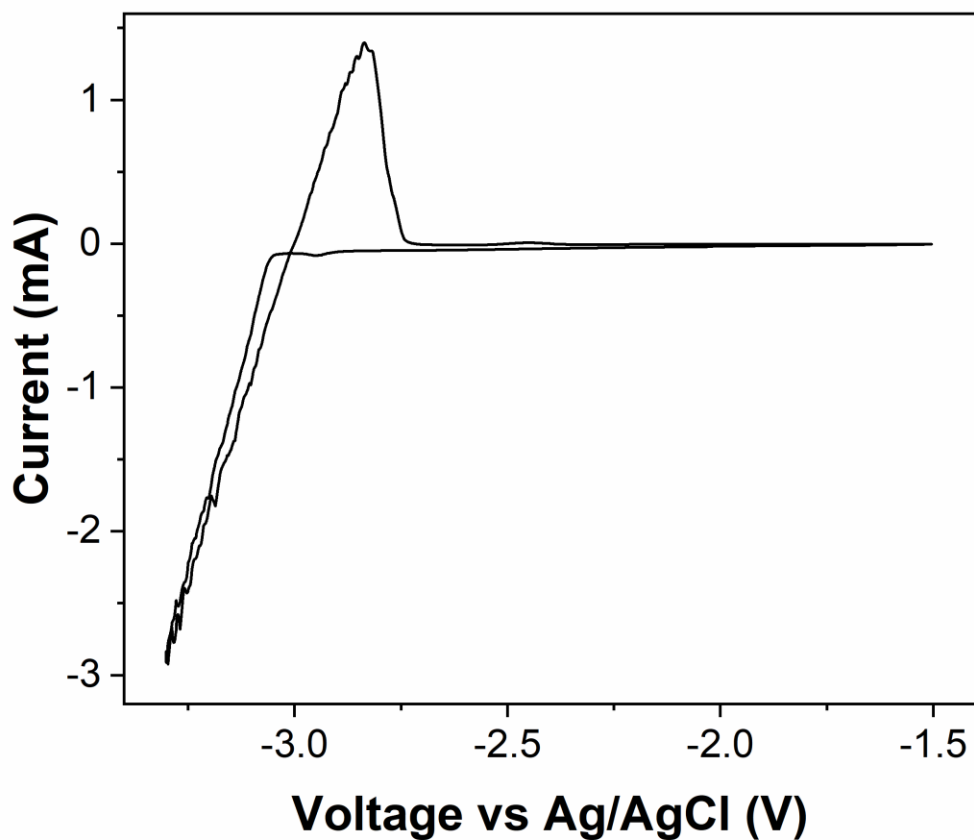


Figure S14. A cyclic voltammogram of a 1 M LiBF₄, 0.2 M EtOH solution in THF, collected at a sweep rate of 5 mV/s with partial resistance compensation. An Ag/AgCl reference was used in a non-aqueous system, which may introduce some error into the absolute values of the potential; it is thus a pseudoreference. Note that no significant current is observed until -3.04 V vs the reference, after which lithium begins to plate. This shows that lithium plating can be assumed to be the initial reaction in the system.

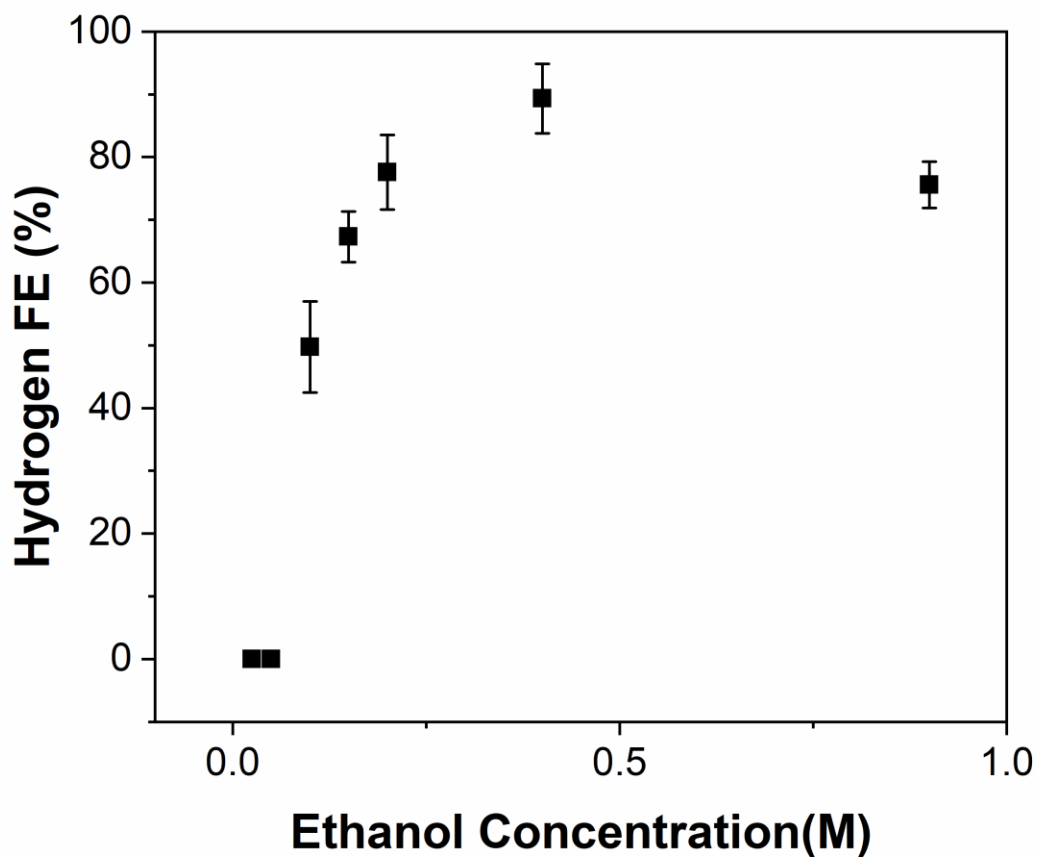


Figure S15. Faradaic efficiency towards hydrogen as a function of ethanol concentration, measured during galvanostatic experiments with an applied current of 3 mA. The FE towards hydrogen is extremely low (undetectable) at low ethanol concentrations (<0.05 M); as the FE for ammonia in this regime is also low, the current goes towards plating lithium, which remains unreacted. At higher concentrations, the FE towards hydrogen begins to increase, reaching close to closure levels above 0.4 M EtOH.

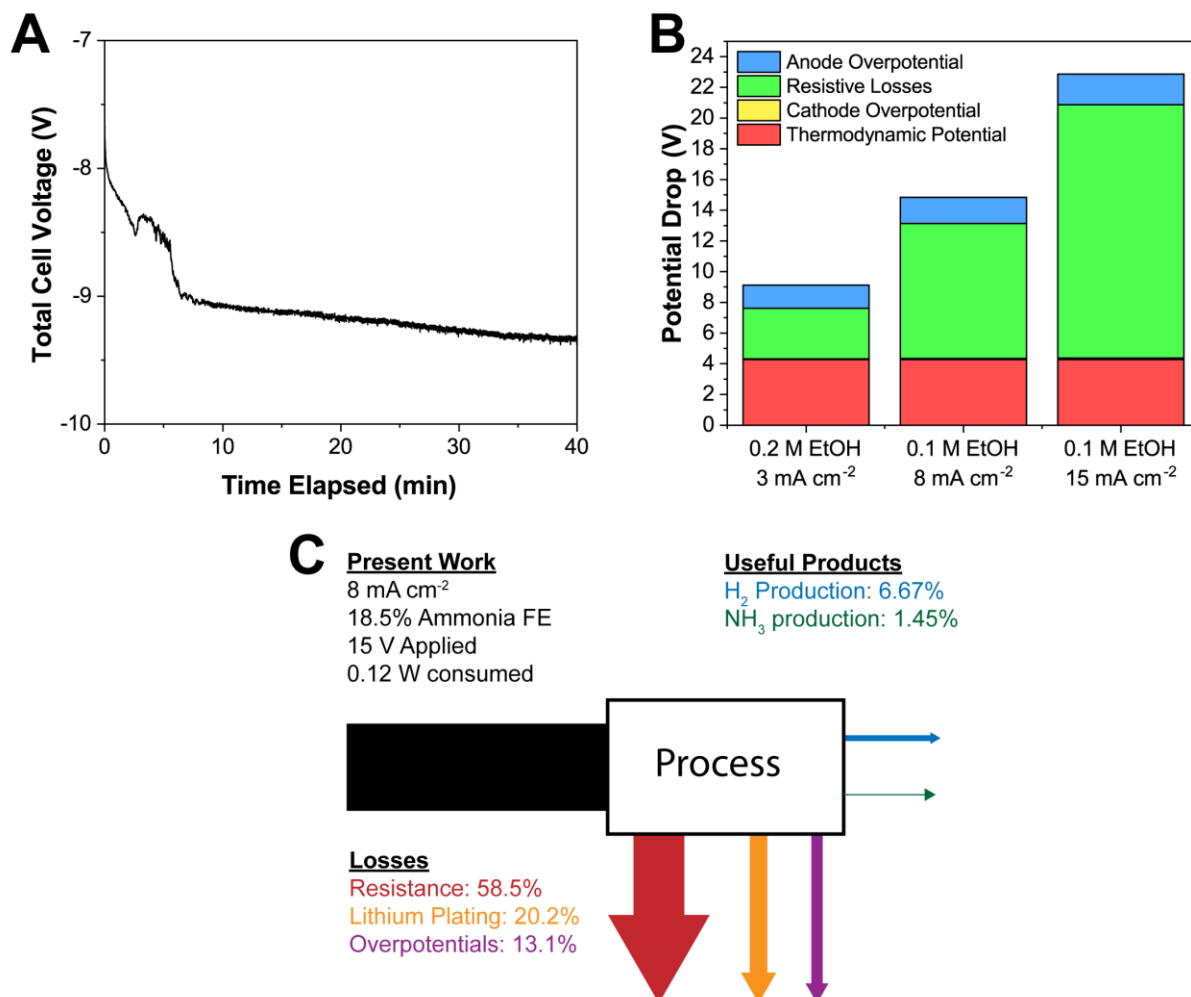


Figure S16. (A) The total cell voltage applied using a typical 0.2 M EtOH, 3 mA cm⁻² experiment. (B) The estimated contributions to the potential drop in a sample of operating parameters. (C) The breakdown of energy losses in a 0.1 M EtOH, 8 mA cm⁻² experiment, where high energy efficiency is achieved.

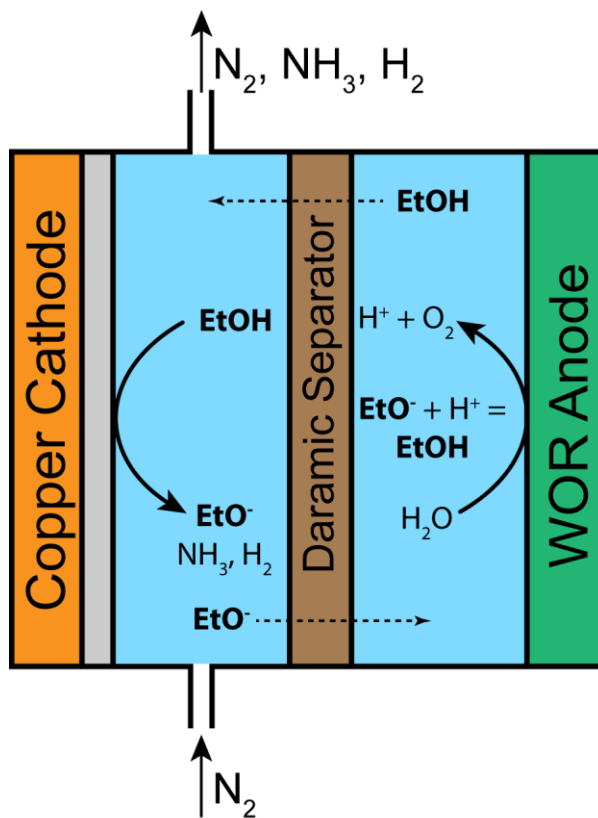


Figure S17. One method proposed to utilize water as the hydrogen source. Water is oxidized at the anode and ferried to the cathode via the proton carrier, depicted here as ethanol. Alternative proton carriers may be used to have greater stability under operating conditions. A similar mechanism for proton motion occurs in many electrochemical systems. In water splitting, protons are generated at the anode and transported by water as H_3O^+ to the cathode, where they are reduced to hydrogen gas.

Literature Summary

Table S1. A selection of reported electrochemical ammonia synthesis methods.

Catalyst	Maximum FE (%)	Maximum Rate (mol cm ⁻² s ⁻¹)	Electrolyte	Conditions	Ref.
Au Nanorods	3.879	2.69×10 ⁻¹¹	0.1 M KOH	5-65 °C, 1 bar	2
Au Nanocages	40.5	6.37×10 ⁻¹¹	0.5 M LiClO ₄ in water	20-50 °C, 1 bar	3
Pd Nanoparticles	8.2	7.35×10 ⁻¹¹	0.1 M PBS	25 °C, 1 bar	4
RuPt Alloy	13.2	1.05×10 ⁻⁹	1 M KOH	50 °C, 1 bar	5
ZIF-coated Ag nanocubes on Au	28	1.50×10 ⁻¹¹	0.2 M Li(CF ₃ SO ₃), EtOH in THF	Ambient	6
γ-Fe ₂ O ₃ Nanoparticles	1.9	1.55×10 ⁻¹¹	0.1 M KOH	65 °C, 1 bar	7
Fe ₂ O ₃ -CNT	0.164	1.06×10 ⁻¹¹	0.5 M KOH	Ambient	8
Fe-FTO	60	2.61×10 ⁻¹¹	[C ₄ mpyr][eFAP], other ionic liquids	20-70 °C, 1 bar	9
Cr ₂ O ₃ microspheres	6.78	4.13×10 ⁻¹⁰	0.1 M Na ₂ SO ₄	Ambient	10
Sm-Fe-Cu-Ni oxide	90.4	1.13×10 ⁻⁸	Nafion (gas diffusion system)	1 bar, 80 °C	11
MoN Nanosheets	1.15	3.01×10 ⁻¹⁰	0.1 M HCl	Ambient	12
VN Nanosheets	2.25	8.40×10 ⁻¹¹	0.1 M HCl	Ambient	13
ZnSe, ZnS	1.29	6.24×10 ⁻⁹	1 M KOH	Ambient	14
Melamine-derived polymeric carbon nitride	11.59	6.61×10 ⁻¹¹	0.1 M HCl	Ambient	15
ZIF-8-derived N-doped carbon	1.42	2.33×10 ⁻¹⁰	0.05 M H ₂ SO ₄	Ambient	16
ZIF-8-derived N-doped carbon	10.2	2.02×10 ⁻⁹	0.1 M KOH	20-60°C	17
B-doped graphene	10.8	1.60×10 ⁻¹⁰	0.05 M H ₂ SO ₄	Ambient	18
N-doped carbon nanospikes	11.56	1.59×10 ⁻⁹	0.25 M LiClO ₄	Ambient	19
Au on nitrogen-doped nanoporous graphitic carbon	22	5.88×10 ⁻¹⁰	0.1 M HCl	Ambient	20
Lithium metal on Fe	59.8	3.99×10 ⁻⁹	0.1 M LiClO ₄ , 0.2 M EtOH in THF	20°C, 50 bar	21
Lithium metal (from LiOH)	88.5	1.06×10 ⁻⁸ (estimated from reported data; process is batch)	Molten LiOH	20-450 °C, 1 bar	22
Lithium metal (from ceramic)	52.3	1.88×10 ⁻⁹ (reported; process is batch)	LISICON ceramic	20-220 °C	23
Lithium metal (concerted nitride formation)	59	1.02×10 ⁻¹⁰ (estimated; ammonia synthesis is batch)	1 M LiCF ₃ SO ₃ in TEGDME	Ambient	24
Lithium metal on Cu	18.5 ± 2.9	(7.9 ± 1.6) × 10⁻⁹	1 M LiBF₄, EtOH, THF	Ambient	This work

Nitrogen Variation Data

Table S2. Faradaic efficiencies towards ammonia as a function of nitrogen partial pressure in triplicate.

Nitrogen Partial Pressure (bar)	Run 1 Faradaic Efficiency (%)	Run 2 Faradaic Efficiency (%)	Run 3 Faradaic Efficiency (%)	Average Faradaic Efficiency (%)
0	-0.11	-0.06	-	-0.08 ± 0.04
0.05	0.15	0.22	0.18	0.18 ± 0.03
0.125	0.42	0.35	0.37	0.38 ± 0.04
0.25	1.39	0.90	1.33	1.21 ± 0.27
0.50	2.92	3.32	2.40	2.88 ± 0.46
0.75	2.87	2.89	3.33	3.03 ± 0.26
1.00	5.74	5.46	5.49	5.56 ± 0.15

Table S3. Ammonia production rates as a function of nitrogen partial pressure in triplicate.

Nitrogen Partial Pressure (bar)	Run 1 Rate (10^{-10} mol cm^{-2} s^{-1})	Run 2 Rate (10^{-10} mol cm^{-2} s^{-1})	Run 3 Rate (10^{-10} mol cm^{-2} s^{-1})	Average Rate (10^{-10} mol cm^{-2} s^{-1})
0	-0.12	-0.06	-	-0.09 ± 0.04
0.05	0.15	0.22	0.19	0.19 ± 0.04
0.125	0.44	0.37	0.38	0.4 ± 0.04
0.25	1.44	0.93	1.38	1.25 ± 0.28
0.50	3.03	3.44	2.49	2.98 ± 0.48
0.75	2.97	2.99	3.45	3.14 ± 0.27
1.00	5.95	5.66	5.69	5.77 ± 0.16

Ethanol Variation Data

Table S4. Faradaic efficiency towards ammonia as a function of ethanol concentration, in triplicate with additional validation runs.

Ethanol Concentration (M)	Run 1 Faradaic Efficiency (%)	Run 2 Faradaic Efficiency (%)	Run 3 Faradaic Efficiency (%)	Additional Runs Faradaic Efficiency (%)	Average Faradaic Efficiency (%)
0.025	0.31	0.17	-0.01	-	0.15 ± 0.16
0.05	4.60	2.09	5.08	-	3.92 ± 1.61
0.10	10.0	3.61	10.1	7.63	7.83 ± 3.04
0.15	4.61	5.24	5.11	-	4.99 ± 0.33
0.20	4.76	3.58	4.81	5.10	4.56 ± 0.67
0.25	3.41	3.19	3.93	-	3.51 ± 0.38
0.40	1.12	1.70	2.46	-	1.76 ± 0.67
0.60	0.89	0.72	0.50	-	0.7 ± 0.2
0.90	0.34	0.37	0.40	-	0.37 ± 0.03
1.50	0.42	0.33	0.14	-	0.3 ± 0.14

Table S5. Ammonia production rate as a function of ethanol concentration, in triplicate with additional validation runs.

Ethanol Concentration (M)	Run 1 Rate (10^{-10} mol cm^{-2} s^{-1})	Run 2 Rate (10^{-10} mol cm^{-2} s^{-1})	Run 3 Rate (10^{-10} mol cm^{-2} s^{-1})	Additional Runs Rate (10^{-10} mol cm^{-2} s^{-1})	Average Rate (10^{-10} mol cm^{-2} s^{-1})
0.025	0.32	0.17	-0.02	-	0.16 ± 0.17
0.05	4.77	2.16	5.27	-	4.06 ± 1.67
0.10	10.37	3.74	10.45	7.91	8.11 ± 3.15
0.15	4.78	5.43	5.29	-	5.17 ± 0.34
0.20	4.94	3.71	4.98	5.28	4.73 ± 0.69
0.25	3.53	3.31	4.08	-	3.64 ± 0.39
0.40	1.16	1.76	2.55	-	1.82 ± 0.69
0.60	0.92	0.74	0.52	-	0.73 ± 0.21
0.90	0.35	0.38	0.42	-	0.38 ± 0.03
1.50	0.44	0.35	0.15	-	0.31 ± 0.15

Current Variation Data

Table S6. Faradaic efficiency towards ammonia as a function of applied current density, in triplicate with additional validation runs.

Current Density (mA cm ⁻²)	Run 1 Faradaic Efficiency (%)	Run 2 Faradaic Efficiency (%)	Run 3 Faradaic Efficiency (%)	Additional Runs Faradaic Efficiency (%)	Average Faradaic Efficiency (%)
0.3	1.56	1.97	1.01	-	1.51 ± 0.48
0.7	1.59	1.85	1.71	-	1.72 ± 0.13
1.5	2.44	2.42	2.47	2.01	2.44 ± 0.22
3	4.66	5.74	5.46	5.49, 5.72	5.29 ± 0.44
6	5.61	9.02	7.23	6.40	7.29 ± 1.46
10	7.53	9.23	7.83	10.55	8.2 ± 1.39
15	7.54	10.11	8.25	12.50	8.63 ± 2.22
19	6.89	8.14	6.83	-	7.29 ± 0.74
22	6.26	6.48	6.04	-	6.26 ± 0.22
25	5.26	6.36	6.10	6.34	5.91 ± 0.52

Table S7. Ammonia production rate as a function of applied current density, in triplicate with additional validation runs.

Current Density (mA cm ⁻²)	Run 1 Rate (10 ⁻¹⁰ mol cm ⁻² s ⁻¹)	Run 2 Rate (10 ⁻¹⁰ mol cm ⁻² s ⁻¹)	Run 3 Rate (10 ⁻¹⁰ mol cm ⁻² s ⁻¹)	Additional Runs (10 ⁻¹⁰ mol cm ⁻² s ⁻¹)	Average Rate (10 ⁻¹⁰ mol cm ⁻² s ⁻¹)
0.3	0.16	0.20	0.10	-	0.16 ± 0.05
0.7	0.38	0.45	0.41	-	0.42 ± 0.03
1.5	1.3	1.3	1.3	1.0	1.3 ± 0.1
3	4.8	5.9	5.7	5.7, 5.9	5.5 ± 0.5
6	11.6	18.7	15.0	13.3	15.1 ± 3.0
10	26.0	31.9	27.0	36.5	28.3 ± 4.8
15	39.1	52.4	42.7	64.8	44.7 ± 11.5
19	45.3	53.5	44.8	-	47.8 ± 4.9
22	47.6	49.2	45.9	-	47.6 ± 1.7
25	45.4	55.0	52.7	57.4	51.0 ± 4.5

Model Validation Experiment Data

Table S8. Ammonia Faradaic efficiencies in experiments associated with coupled kinetic-transport model validation.

Operating Conditions	Run 1 Faradaic Efficiency (%)	Run 2 Faradaic Efficiency (%)	Run 3 Faradaic Efficiency (%)	Average Faradaic Efficiency (%)
0.1 M EtOH, 8 mA cm ⁻²	20.52	15.20	19.92	18.54 ± 2.91
0.1 M EtOH, 15 mA cm ⁻²	15.94	17.91	11.78	15.2 ± 3.13

Table S9. Ammonia production rates in experiments associated with coupled kinetic-transport model validation.

Operating Conditions	Run 1 Production Rate (10 ⁻⁹ mol cm ⁻² s ⁻¹)	Run 2 Production Rate (10 ⁻⁹ mol cm ⁻² s ⁻¹)	Run 3 Production Rate (10 ⁻⁹ mol cm ⁻² s ⁻¹)	Average Production Rate (10 ⁻⁹ mol cm ⁻² s ⁻¹)
0.1 M EtOH, 8 mA cm ⁻²	5.67	4.20	5.50	5.12 ± 0.81
0.1 M EtOH, 15 mA cm ⁻²	8.26	9.28	6.10	7.88 ± 1.62

Supplemental Experimental Procedures

Materials

Tetrahydrofuran (C₄H₈O, 99+%, stabilized with BHT) and molecular sieves (3Å, 4-8 mesh) were purchased from Acros Organics. Lithium tetrafluoroborate (LiBF₄, 98%), sodium salicylate (C₆H₄(COONa)(OH), *ReagentPlus*®, ≥99.5%), sodium hypochlorite (NaOCl, reagent grade, 10-15% available chlorine), hydrochloric acid (HCl, ACS reagent, 37%), and FeCl₃·6H₂O (ACS Reagent, 97%) were purchased from Sigma-Aldrich. Alternative vendors (AV) for LiBF₄ tested included Alfa Aesar (98%), TCI America, and Beantown Chemical (≥98%). Copper foil (Cu, 99.9%, 0.025 mm thick) was purchased from Strem Chemical Inc. The alternative vendor for copper foils tested was Alfa Aesar (0.025 mm, annealed, uncoated, 99.8%). Platinum foil (Pt, 0.025 mm thick, 99.99%, trace metals basis) was purchased from Beantown Chemical. Ethyl alcohol (C₂H₅OH, Koptec, anhydrous, 200 proof), sodium hydroxide (NaOH, Macron Fine Chemicals, pellet form), and acetone (ACS, BDH Chemical) were purchased from VWR International. Nitric acid (HNO₃, 67-70%, trace metal grade), sulfuric acid (H₂SO₄, 93-98%, trace metal grade), and diethyl ether (C₄H₁₀O, laboratory grade) were purchased from Fisher Scientific. Sodium nitroprusside (Na₃[Fe(CN)₅(NO)]·2H₂O, sodium pentacyanonitrosylferrate (III) dihydrate, 99-102%), ferrocene (99%, powder), NH₄PF₆ (99.5%, powder), were purchased from Alfa Aesar. Isotope labelled nitrogen (¹⁵N₂, 98%+) was purchased from Cambridge Isotope Laboratories, Inc. Argon gas (UHP, 5.0 grade) was purchased from Airgas. N₂ gas was available in-house and was generated by boiloff of liquid nitrogen from Airgas. Polyporous Daramic 175 separators were received as a sample from Daramic (Charlotte, NC). PTFE membrane filters (47 mm, 0.22 μm pore size) were purchased from Tisch Scientific. 400 grit sandpaper (Norton Blue Bak, waterproof) and 1500 grit sandpaper (G2, waterproof, Finish 1st) were purchased from W.W. Grainger Inc.

Preparation of Electrolyte Solutions

Molecular sieves were activated by washing with acetone and heating in a furnace at 350°C for 4 hours. They were then cooled to room temperature and stored in an airtight container. Tetrahydrofuran was dried by adding approximately 20% v/v of activated molecular sieves to the solvent in a round bottom flask. The flask was then sealed from the atmosphere with a rubber stopper and kept away from light. The tetrahydrofuran was found to be sufficiently dry for nitrogen reduction after 48 hours of drying, but optimal dryness was obtained after at least 96 hours of drying.

Lithium tetrafluoroborate was dissolved in dry tetrahydrofuran in a centrifuge tube to obtain a 1M solution of LiBF₄ in THF. Ethanol was added to this solution to obtain the desired concentration of proton source. The solution was then centrifuged to remove undissolved residue. The clear solution was transferred and stored in oven-dried glass vials and used within 12 hours of preparation.

LiBF₄ Purification

The lithium tetrafluoroborate must be dry and pure to obtain good results. The reagent purchased from Sigma-Aldrich was found to be sufficiently pure and dry for ammonia production experiments. LiBF₄ from alternative vendors was not found to be pure enough. A method to purify these salts was developed in order to improve ammonia yields, which is described below.

Unpurified LiBF₄ was dissolved in water to make a saturated aqueous solution of LiBF₄ (the solubility was found to be approximately 95 g of LiBF₄ per 100 g of water). The saturated solution was centrifuged multiple times to remove all undissolved material (typically black or orange precipitates). The clear saturated solution was then cooled to -20°C to form lithium tetrafluoroborate hydrate crystals. The mother liquor was removed from the crystals via pipetting. This must be done quickly, as the crystals can melt back into solution form. The crystals were then dried under vacuum at 40°C for 16 h. During this process, they may melt, but will release most of the held water. Alternatively, one could freeze dry the crystals to prevent melting. The dried crystals were then crushed, and the resulting powder was washed twice with diethyl ether (the solubility of LiBF₄ in ethyl ether is 1.3 g per 100 mL).²⁵ The resulting powder was then dried at 110°C under vacuum for 16 hours. The resulting dry, purified LiBF₄ was stored under an inert atmosphere and demonstrated satisfactory ammonia yields in nitrogen reduction experiments (Figure S10).

Cathode Preparation

Polished copper was used as the cathode substrate material. A piece of foil approximately 15 mm by 15 mm was used in a cell. To prepare the foil, the metal was wet with deionized water and polished with 400 grit sandpaper, followed by 1500 grit sandpaper. The polished foil was then rinsed with deionized water again, dipped into a 5% nitric acid solution for 10-15 seconds, and thoroughly rinsed with deionized water to remove any nitric acid or nitrate residue. It was dried for at least 15 minutes at 80°C before use.

Nitrogen Reduction Experiments

The electrochemical experiments were performed using a 2-compartment cell (Figure S1, Figure S2). A polished copper foil was used as the cathode; a platinum foil was used as the anode. Due to the design of the cell, the active area of the electrodes is 1 cm². A piece of Daramic 175 separated the anode and cathode compartments of the cell. A platinum wire was inserted into the cathode compartment to act as a pseudo-reference for resistance and potential measurements. All cell parts (including the electrodes and separator) were washed with deionized water to remove any contamination and oven dried at 80°C for at least 20 minutes prior to cell assembly to remove any residual moisture. 1.75 mL of prepared LiBF₄/EtOH/THF electrolyte solution was added to each chamber. N₂ gas, which was saturated with THF by flowing it through a bubbler filled with the solvent (Figure S2), was delivered to the cathode compartment at a rate of 10 sccm. The flowrate was set by using an Alicat flow controller.

Prior to polarization, the cathode compartment was purged with a THF-rich nitrogen stream for at least 10 minutes. Afterwards, lithium was plated galvanostatically onto the copper cathode. In a typical experiment, 3 mA of current was applied to an electrode with 1 cm² of exposed area using a Biologic VMP3 potentiostat for 40 minutes, unless the effects of current density were being studied. After polarization, the catholyte was removed from the cell and immediately diluted with water to neutralize any free lithium remaining and to prepare the solution for quantification. Typically, 200 μL of catholyte were added to 1800 μL of deionized water; however, less catholyte was added to more water in some experiments (50, 100 μL to 1950, 1900 μL respectively) if the anticipated amount of ammonia produced would lie outside the quantification calibration curve.

In experiments where the effects of current density were studied, 1M LiBF₄, 0.2 M EtOH in THF solutions were used. There were minor differences in experiments run at low (<5 mA cm⁻²) and high (>5 mA cm⁻²) current densities. At low current densities, current was applied for 40 minutes using a Biologic VMP3 potentiostat regardless of current density. A constant running time was chosen to mitigate the effects of diffusion of ammonia through the separator for longer experiments (Figure S11). At high current densities, a constant 7.2 coulombs (the amount of charge passed at 3 mA over 40 minutes) of charge was supplied using a Tekpower TP3005T DC power supply. A constant charge was passed to allow us to assume a constant ethanol concentration in all experiments, as only ~10% of the ethanol will have reacted; longer times could cause much of the ethanol to react with lithium, lowering its concentration over time.

Control Experiments

The experiments depicted in Figures 3, 4, and 5 were performed as described above. The control experiments depicted in Figure 2 were performed with modifications due to the high cost of ¹⁵N₂. In these experiments, the setup was analogous to the one depicted in Figure S2B, albeit a smaller volume THF bubbler was used to decrease the residence time of gas in the bubbler. The cell was initially purged with argon at 10 sccm for 5 minutes to remove oxygen and ¹⁴N₂ from the electrolyte solution. After purging, ¹⁵N₂, ¹⁴N₂, or Ar was used as the feed gas depending on the experiment. The gas was bubbled through the cell at 5 sccm for 5 minutes. Then, either the cell was held at OCV or 15 mA of current were applied to the cell while maintaining the flowrate of 5 sccm for 15 minutes. Control experiments with no applied current are imperative for isotope labelled experiments, as there have been reports of ammonia contamination in ¹⁵N₂ stocks.²⁶ If ammonia is detected in experiments where no potential is applied, then the gas is contaminated and should be purified by bubbling through an acidic bubbler.⁹ The electrolyte was removed from the cell after the experiment. Part of the electrolyte was quenched by diluting 100 μL of it in 1900 μL of DI water to quantify the ammonia content of the electrolyte using the salicylate method. The remaining electrolyte solution was diluted in a 1:1 ratio with 0.5 M H₂SO₄. This converts any ammonia present to the ammonium (NH₄⁺) form. The NMR spectra were measured on a Varian Inova-500 instrument with solvent suppression of the three largest peaks (1 from H₂O, 2 from THF).

Figure 2A was made by running a typical cell as described in “Nitrogen Reduction Experiments.” 0.2 M EtOH electrolyte was used and 3 mA of current was applied. Aliquots of the catholyte (40 μ L at a time) were taken out of the cell and diluted in 2000 μ L of water for quantification using the salicylate method. 40 μ L of fresh electrolyte were added to the cell to replace the removed electrolyte.

Ammonia Quantification

Ammonia in water-quenched THF samples was quantified by using a modification of the salicylate method.²⁷ The following stock solutions were made for quantification:

Salicylate solution: 40 g of sodium salicylate was transferred to a 100 mL volumetric flask. 50 mL of DI water was added to partially dissolve the solid. 1 mL of 0.05 M sodium nitroprusside, made by dissolving 149 mg of $\text{Na}_2[\text{Fe}(\text{CN})_5\text{NO}] \cdot 2\text{H}_2\text{O}$ in 10 mL of DI water, was added to the flask, followed by DI water until all solids dissolved. The solution was then diluted to the mark with DI water to obtain a solution containing 2.5 M sodium salicylate and $5 \cdot 10^{-4}$ M sodium nitroprusside. The solution was stored in the dark at 5°C and was stable for approximately 3 months.

Sometimes, the sodium salicylate was found to contain unacceptable amounts of ammonia contamination which made it difficult to accurately quantify small amounts of produced ammonia. In this case, the preparation procedure was modified slightly. 40 g of sodium salicylate was dissolved in 300 mL of DI water. 50 mL of 6M HCl were added dropwise to form a white salicylic acid precipitate. The precipitate was filtered from the water and washed with DI water multiple times to remove acid and salt remains. The salicylic acid was dried under vacuum at 40°C for 3 hours to obtain an accurate measurement of the dry mass. The yield in this step is usually >90%, limited only by transfer losses and slight solubility of salicylic acid in water. For every 10 g of dry salicylic acid, 17.5 mL of 4M NaOH was added. Residual salicylic acid was removed by centrifugation. 290 μ L of 0.05 M sodium nitroprusside was added to the solution, and solution was diluted to 29 mL with DI water.

Alkaline solution: 800 mg of sodium hydroxide was dissolved in 50 mL of DI water to obtain 0.4 M NaOH. The solution was stored at 5°C and was stable indefinitely if sealed from the atmosphere.

An alkaline solution of ~1% hypochlorite was made just prior to quantification by mixing 10-15% NaOCl and 0.4 M NaOH in a 1:9 volume ratio. Stock salicylate solutions were made beforehand.

A typical ammonia sample had a volume of 2000 μ L. To a typical sample 280 μ L of the fresh hypochlorite solution and 280 μ L of the salicylate solution were added in that order. The resulting solution was thoroughly mixed and left to react in the dark for approximately 2 hours. The solution absorbance spectrum was then measured with an Ocean Optics spectrophotometer with a Flame-S-UV-Vis detector and a DH-mini-UV-Vis-NIR light source.

A new calibration curve was made every time a batch of samples was measured (Figure S5). Calibration solutions were made by adding 200 μ L (or another volume, if samples were made by diluting a different volume of electrolyte in water) of unused $\text{LiBF}_4/\text{EtOH}/\text{THF}$ electrolyte to 1800 μ L of 0 μ M, 20 μ M, 40 μ M, and 80 μ M NH_4^+ standards. The electrolyte used to prepare calibration solutions is identical to one used in N_2 reduction experiments; it contains all the same potential contaminants that are could be present in ammonia samples.

As no ammonia was produced in typical experiments where Ar was used as a feed gas (Figure 3, Table S2), the ammonia Faradaic efficiency and production rate were computed directly from measured concentrations. This is consistent with recommended quantification and reporting procedures in the literature.²⁸ The Faradaic efficiency for ammonia was computed as follows:

$$FE(\text{NH}_3) = C_{\text{NH}_3} \cdot \frac{V}{I \cdot t \cdot 3F}$$

Boundary Layer Thickness Measurement

In order to obtain an estimate of the transport-limited current density, the boundary layer thickness was computed by measuring the limiting current density for the reduction of ferrocenium hexafluorophosphate ($[\text{Fc}^+][\text{PF}_6^-]$). $[\text{Fc}^+][\text{PF}_6^-]$ was synthesized from ferrocene and NH_4PF_6 using a method described in the literature.²⁹ To a typical electrolyte solution (1 M LiBF_4 , 0.2 M EtOH in THF), 2 mM of

[Fc⁺][PF₆⁻] was added. This spiked solution was used as the electrolyte in the same cell that was used in nitrogen reduction experiments; 10 sccm of nitrogen was fed to the cell, as in nitrogen reduction experiments. A sufficiently negative constant potential above the lithium plating potential was applied (between -2.0 V and -3.0 V vs Ag/AgCl) in order to reach the transport limited current for ferrocenium reduction (Figure S8).

Side Product Quantification

In lithium-mediated nitrogen reduction experiments, hydrogen is the main gaseous side product, while lithium metal and lithium nitride are potential side products that may be generated as solids on the cathode surface. In order to quantify the hydrogen FE, the gas stream that passed through the cathode compartment during polarization was bubbled through water to capture THF vapors and fed to an SRI Instruments Gas Chromatograph (GC, SRI 8610C) (Figure S2). Nitrogen gas was used as the GC carrier gas and a thermal conductivity detector was used to measure the signal. The hydrogen peaks area was used to quantify hydrogen using a calibration curve.

In order to quantify lithium nitride, the cell was disassembled, and the copper foil with solids on it was removed. The foil was dipped into 5 mL of 0.1 M HCl to dissolve lithium nitride and lithium metal. Before quantification, 1500 μ L of the resulting acidic solution was mixed with 500 μ L of 0.4 M NaOH, after which typical salicylate quantification was performed.

Separator Permeability Measurements

Two separator materials were tested in the electrochemical cell to show the impact of ammonia diffusion in the cell: Daramic 175 and the membrane from PTFE filter paper (0.22 μ m, Tisch Scientific) (Figure S11). To measure the diffusion rate of ammonia across the separator, a typical electrochemical cell was assembled with no gas flow. A solution of 1 M LiBF₄, 0.2 M EtOH in THF was added to both compartments. 35 μ L of 0.01 M NH₄OH in water was added to one of the compartments (denoted “counter”, even though no electrochemistry was performed). The cell was left without polarization for a given amount of time, after which the solution from each compartment was extracted and diluted 10-fold in water. The ammonia concentration in the diluted solutions was then quantified using the salicylate method. From the difference in concentration of ammonia in the two compartments, the diffusion rate of ammonia through the separator was estimated.

Analysis of Absorbance

While the absorbance of the resulting solutions at a given wavelength can directly be used to compute the concentration of ammonia, we elected to use a modified metric as the signal. The difference between absorbance values at 475 nm (arbitrarily chosen) and 650 nm (salicylate indophenol peak absorbance wavelength) was used as the signal to compute the amount of ammonia present (Figure S3). This method of obtaining the ammonia signal can eliminate baseline shifts that sometimes occur due to the fiber-optic design of the Ocean Optics spectrophotometer. In addition, it significantly diminishes the chances of overestimating the concentration of ammonia due to turbidity of solutions.

If a baseline shift of A_0 is assumed to be present at all wavelengths, then it is eliminated if the metric described previously is used as the signal:

$$A_{475} = A_{475,true} + A_0 = \epsilon_{475}Cl + A_0 \quad (1)$$

$$A_{650} = A_{650,true} + A_0 = \epsilon_{650}Cl + A_0 \quad (2)$$

$$S = A_{650} - A_{475} = \epsilon_{650}Cl + A_0 - (\epsilon_{475}Cl + A_0) = (\epsilon_{650} - \epsilon_{475})Cl \quad (3)$$

A_x is the absorbance at a given wavelength, ϵ_x is the extinction coefficient from Beer’s law at a given wavelength. C is the concentration of indophenol formed from ammonia, and l is the light pathlength. The value of $(\epsilon_{650} - \epsilon_{475})l$ can be obtained from the calibration curve.

If a solution is slightly cloudy, some light scattering may occur. Assuming Rayleigh scattering, the effective absorbance is given by $A_\lambda = \sigma\lambda^{-4}$.³⁰ A scattering solution can increase the absorbance at the wavelength of interest, and lead to overestimation of the concentration of ammonia present. By using the difference between the absorbance at two wavelengths, this bias can be eliminated:

$$\begin{aligned}
A_{475} &= A_{475,true} + A_{475,scatter} = \epsilon_{475}Cl + \sigma(475)^{-4} \\
A_{650} &= A_{650,true} + A_{650,scatter} = \epsilon_{650}Cl + \sigma(650)^{-4} \\
S &= A_{650} - A_{475} = \epsilon_{650}Cl + \sigma(650)^{-4} - (\epsilon_{475}Cl + \sigma(475)^{-4}) = \\
&(\epsilon_{650} - \epsilon_{475})Cl + \sigma(650^{-4} - 475^{-4}) < (\epsilon_{650} - \epsilon_{475})Cl
\end{aligned}$$

In fact, we see that this will lead to underestimation of the concentration of ammonia in solution. While this method still may not give accurate ammonia concentrations in turbid solutions, it at least avoids wrongly attributing increased absorbance to a higher concentration of ammonia; i.e. it avoids false positives and overestimation of yields.

Calculation of N₂ Transport Limited Current Density

We took the limiting current density of ferrocenium reduction to be 0.45±0.05 mA cm⁻² from experiment (Figure S8). In order to find the boundary layer thickness, the diffusion coefficient of ferrocenium (F_{cm}) in the electrolyte solution must be known:³¹

$$\delta = \frac{C_{Fcm}D_{Fcm}F}{J_{lim}}$$

This equation is valid despite the fact that ferrocenium is charged and may experience migration in addition to diffusion, as a large concentration of supporting electrolyte is used. We were not able to find literature values for the diffusion coefficient of ferrocenium in 1 M LiBF₄/THF electrolyte. Therefore, we estimated the diffusion coefficient by using known values in other solvents and the Stokes-Einstein equation:^{32,33}

$$D_i = \frac{kT}{6\pi r_i \eta}$$

We were unable to find the exact viscosity of LiBF₄/THF solutions in the literature, and therefore used values found for LiClO₄/THF solutions of similar concentrations.³⁴ We assumed the viscosity to be 0.75 ± 0.1 cP at 25°C. The hydrodynamic radius can be eliminated from calculations as we assume it is constant between solvents. Based on this, we estimate the diffusion coefficient of ferrocenium in our electrolyte to be 1.2 ± 0.3·10⁻⁹ m² s⁻¹. This implies that diffusion boundary layer thickness is approximately 50 ± 15 µm.

In order to estimate the limiting current density for nitrogen reduction, the solubility and diffusivity of nitrogen in the electrolyte solution must be known. The diffusivity can be estimated using known values in other solvents³⁵⁻³⁷ and the Stokes-Einstein equation, and was assumed to be 2.5 ± 1.0·10⁻⁹ m² s⁻¹. The tabulated solubility of nitrogen in THF is 6.2 mM.^{38,39} However because of the “salting-out” effect, the solubility of gases in solvents decreases with increasing salt concentration.⁴⁰ We were not able to find studies that measure nitrogen solubility in THF as a function of electrolyte concentration; hence, we estimated the magnitude of salting out from other data. From information that the salting-out effect could almost half the solubility of O₂, a gas similar to N₂, in electrolyte-containing DMSO solutions,⁴¹ we assumed that a similar decrease in nitrogen solubility could be possible in our system. The nitrogen solubility was estimated to be 4 ± 2 mM. In this case, the limiting current density for nitrogen reduction would be 11.6 ± 8.0 mA cm⁻². The predicted limiting current density from the partial current density at the peak Faradaic efficiency is 3.9 ± 0.9 mA cm⁻², which lies within the (fairly large) error bars of our nitrogen reduction limiting current density estimate.

Derivation of Nitrogen Transport Limited Peak FE Expression

We mentioned in the Discussion of the main text that it is possible to show that ammonia FE is maximized when the partial current density towards ammonia is one third of the transport limited current density. While this result can be obtained by directly taking the derivative with respect to applied current density of the FE expression (Eq. 12), we present a simpler approach below. From Eq. 11, we can see that the FE is maximized when

$$[Li]^{\beta-\alpha}[N_2] = \frac{C_{bulk}[Li]^{\beta-\alpha}}{1 + \frac{\delta}{6FD}k_2[Li]^\beta}$$

is maximized. By taking the derivative of the above expression with respect to $[Li]$ and setting it to zero, we find an expression that is valid when the ammonia FE is maximized:

$$[Li]^\beta = \left(\frac{\beta - \alpha}{\alpha}\right) \cdot \frac{6FD}{\delta k_2}$$

The concentration of nitrogen at the electrode surface when FE is maximized is given by:

$$[N_2]_{peak} = \frac{C_{bulk}}{1 + \frac{\beta - \alpha}{\alpha}} = \frac{2}{3} C_{bulk}$$

As the transport limited current is given by⁴²

$$I_{lim} = \frac{6DF}{\delta} C_{bulk}$$

We find that the partial current density towards ammonia at which ammonia FE is maximized is:

$$I_{peak} = \frac{6DF}{\delta} \left(C_{bulk} - \frac{2}{3} C_{bulk} \right) = \frac{I_{lim}}{3}$$

Comparison of Models

In order to verify and compare kinetic models (Figure 6), constant parameters were grouped together for simplicity. The values of these grouped constant parameters were found by fitting using experimental results obtained at 0.2 M EtOH, 15 mA cm⁻², and 1 bar N₂ experimental conditions (FE = 8.63%). In all models, $\alpha = 2$ and $\beta = 3$ were assumed, the pressure was taken in units of bar, the current density in units of mA cm⁻², and the ethanol concentration in units of mol L⁻¹. In the case of the simple kinetic model (Eq. 7), the model was simplified to:

$$FE_{NH_3} = A \frac{[N_2] I^{0.5}}{[EtOH]^{1.5}}$$

The value of A was found to be 0.1993, assuming aforementioned units.

In the case of finite lithium concentration model, the model was simplified to:

$$[Li] = \max\left(8.66, \frac{I^{0.5}}{[EtOH]^{0.5}}\right)$$

$$FE_{NH_3} = \frac{A[N_2][Li]^3}{I}$$

The value of 8.66 as the maximum lithium concentration was determined by using 0.2 M EtOH, 15 mA cm⁻² as the conditions when the maximum concentration is obtained, assuming aforementioned units are used.

The coupled kinetic-transport model (Eq. 12) was simplified to:

$$FE_{NH_3} = \frac{I^{0.5}}{[EtOH]^{1.5}} \cdot \frac{A}{1 + B \frac{I^{1.5}}{[EtOH]^{1.5}}}$$

In order to fit two constants, in addition to matching the FE value at 0.2 M EtOH, 15 mA cm⁻², we impose an additional constraint defining this point as the point of maximum FE:

$$\left. \frac{dFE_{NH_3}}{dI} \right|_{0.2 M, 15 mA cm^{-2}} = 0$$

Using these constraints, we found A and B to have values of 0.299 and 7.70×10⁻⁴ respectively.

Effect of a Good Separator

We found that produced ammonia can quickly be oxidized at the platinum anode, especially if the cell is built without a separator between the anode and cathode compartments. This was observed in a typical cell built without a separator (Figure S11A). 1 M LiBF₄, 0.2 M EtOH, THF electrolyte was added to the cell which was spiked with 90 μM NH₄OH. After applying 2 mA of current through the cell for 3 minutes, the concentration of ammonia decreased significantly. As no ammonia was detected in the effluent gas stream, we concluded that the ammonia was oxidized at the platinum anode.

In order to prevent bulk convection of ammonia towards the anode, a separator must be used. However, thin separators must be avoided (Figure S11B-D). In a cell built with a PTFE filter membrane, which is approximately 7 μm thick, as a separator, ammonia quickly diffuses between compartments. Ammonia is added to the anode compartment, and the cell is allowed to remain at OCV to measure the diffusion of ammonia through the separator. The ammonia concentrations in the anode and cathode compartments fully equalize after 2 hours of rest. After 20 minutes of rest, approximately 50% of the ammonia has diffused between compartments. Because of the fast rate of diffusion of ammonia through this separator, the measured concentration in the cathode compartment after nitrogen reduction experiments could be lower than expected. When Daramic 175, which is 175 μm thick, was used as the separator, the two compartments are not equilibrated even after 3 hours of rest (Figure S11E). After 40 minutes, approximately 10% of the ammonia has diffused through the Daramic separator (Figure S11F). Thus, the ammonia measured in the cathode compartment can be assumed to be representative of the amount of ammonia produced.

Estimation of Energy Efficiency

In order to determine the viability of this approach for ammonia synthesis in the future, the energy efficiency of the current process was estimated. First, the potential drop contributions in a typical experiment were measured or estimated. The voltage drop defined by the thermodynamics of the electrochemical reactions was assumed to be 4.27 V: lithium plating is -3.04 V vs SHE and the anode reaction is assumed to be +1.23 V vs SHE. The oxidation reaction at the anode is assumed to have the same thermodynamic potential as water oxidation; this is a conservative estimate for the potential of the anode reaction.²² The voltage drop from resistive dissipation was estimated by $V = IR$; the resistance in the cell was measured by performing a potentiostatic impedance spectroscopy experiment over the entire cell and was found to be ~1100 Ω. From measured cathode potentials, the overpotential for lithium plating was estimated and found to be quite small, while the overpotential for the anode reaction was large (Figure S15). The anode overpotential was estimated by subtracting the resistive losses, thermodynamic potential, and lithium overpotential from the total applied voltage.

The energy efficiencies for hydrogen and ammonia production were estimated by dividing the free energy obtainable from the products viable oxidation by the energy put into the cell:

$$\eta_{NH_3} = \frac{E_{NH_3} \cdot I_{NH_3}}{U_{total} \cdot I_{total}} = \frac{1.18V \cdot I_{NH_3}}{U_{total} \cdot I_{total}}$$
$$\eta_{H_2} = \frac{E_{H_2} \cdot I_{H_2}}{U_{total} \cdot I_{total}} = \frac{1.23V \cdot I_{H_2}}{U_{total} \cdot I_{total}}$$

The fraction of energy lost to various sources was estimated by dividing the excess potential drop required for that source by the total potential drop in the cell. For instance, the fraction of energy lost to thermodynamic inefficiencies (i.e. due to plating lithium) was $\frac{4.27 - (1.18)V}{U_{total}}$, where 4.27 V and 1.18 V are the thermodynamic potentials for the $4Li^+ + 2H_2O \rightarrow 4Li + O_2 + 4H^+$ and $2N_2 + 6H_2O \rightarrow 4NH_3 + 3O_2$ reactions respectively. The fraction of energy lost to overpotentials is defined by $\frac{\eta_{cat} + \eta_{an}}{U_{total}}$. The fraction of energy lost to resistive dissipation was computed by $\frac{IR}{U_{total}}$.

Common Mistakes to Avoid in Experimental Procedures

Over the course of this work, a number of factors were found to negatively affect ammonia yields. In order to achieve high and reproducible yields, it is important to avoid certain mistakes, listed below:

- **Not using a separator between anode and cathode chambers.** Ammonia was found to easily oxidize at the platinum anode; a separator can prevent this.
- **Not using a thick enough separator.** While a separator significantly increases measured Faradaic efficiency towards ammonia, ammonia can diffuse through thin separators, leading to irreproducible yields. Daramic 175, a polyporous separator, was found to be thick enough to prevent diffusion. Other common battery separators (e.g. Celgard 3501) can work, but do not work as well as Daramic.
- **Not drying electrolyte solutions.** Small amounts of water in the LiBF_4 and THF can negatively affect ammonia yields. THF, in particular, must be dried over molecular sieves.
- **Not drying cell parts.** Similar to the electrolyte solutions, all cell parts (electrodes, current collectors, separator, reference, actual cell) must be dried to remove residual water.
- **Using impure LiBF_4 .** Many vendors sell impure LiBF_4 ; LiBF_4 from Sigma-Aldrich was found to be clean and dry enough for these experiments to be used without further purification. Unclean LiBF_4 typically has a yellowish tint in solution, forms black precipitates upon centrifuging, and significantly impacts ammonia yields. A purification procedure for LiBF_4 from alternative vendors was developed to somewhat improve Faradaic efficiency towards ammonia.
- **Using unstabilized THF.** In this work, THF stabilized with BHT was used, which prevents formation of organic peroxides when exposed to air. Unstabilized THF can be used successfully to synthesize ammonia; the salicylate method used for quantification, however, is affected by organic peroxides. The absorbance of indophenol decreases in the presence of peroxides, making it difficult to correctly estimate the ammonia yields. By carefully controlling exposure of THF to air, peroxide formation can be prevented. We, however, recommend using THF stabilized with BHT due to ease of use.
- **Keeping sieves in electrolyte solutions.** The electrolyte solutions work best when used within 12 hours of preparation. If solutions are not stored over sieves, water can enter them from the environment over time. If sieves are present in the solution, they sometimes induce formation of crystals and generally lead to very poor ammonia yields. In either case, using fresh solutions helps improve yields.
- **Not diluting the ammonia-containing electrolyte with water immediately.** When the electrolyte solution is taken out of the cell, it should be immediately (i.e. within 5 minutes) diluted with water to make samples for quantification. The electrolyte solution contains a small amount of residual lithium metal, as well as dissolved nitrogen. These can react over time to form a small amount of additional ammonia that was not made during electrolysis, which can increase the apparent Faradaic efficiency of the process. However, as this additional ammonia is not generated during the electrolysis, it is not correct to include it in Faradaic efficiency and production rate calculations. In addition, if the time before quenching is different, the apparent increase in ammonia concentration can differ in magnitude, which can lead to irreproducible yields.
- **Not adding solutions simultaneously when quantifying ammonia.** In the salicylate method described above, the alkaline hypochlorite solution is added to a sample, followed by the salicylate solution. If the salicylate solution is not added within ~1 minute of adding the hypochlorite solution, the absorbance of the solution can decrease and lead to irreproducible measurements.
- **Reusing copper foils.** The performance of the copper foils was found to deteriorate after reuse, even after repolishing. Fresh copper should be used when preparing the cathode.
- **Using impure copper foils.** 99.9% copper foils, as described in the Materials section, were used in this work and result in high ammonia yields. Thicker copper foils of 99.8% purity were found to result in slightly lower ammonia yields, which suggests a yet unstudied effect of the substrate on nitrogen reduction.

Supplemental References

- [1] Lobaccaro P, Singh MR, Clark EL, Kwon Y, Bell AT, Ager JW. Effects of temperature and gas-liquid mass transfer on the operation of small electrochemical cells for the quantitative evaluation of CO₂ reduction electrocatalysts. *Phys. Chem. Chem. Phys.* **2016**, *18*:26777–85. doi:10.1039/C6CP05287H.
- [2] Bao D, Zhang Q, Meng F-L, Zhong H-X, Shi M-M, Zhang Y, et al. Electrochemical Reduction of N₂ under Ambient Conditions for Artificial N₂ Fixation and Renewable Energy Storage Using N₂/NH₃ Cycle. *Adv. Mater.* **2017**, *29*:1604799. doi:10.1002/adma.201604799.
- [3] Nazemi M, Panikkanvalappil SR, El-Sayed MA. Enhancing the rate of electrochemical nitrogen reduction reaction for ammonia synthesis under ambient conditions using hollow gold nanocages. *Nano Energy* **2018**, *49*:316–23. doi:10.1016/j.nanoen.2018.04.039.
- [4] Wang J, Yu L, Hu L, Chen G, Xin H, Feng X. Ambient ammonia synthesis via palladium-catalyzed electrohydrogenation of dinitrogen at low overpotential. *Nat. Commun.* **2018**, *9*:1795. doi:10.1038/s41467-018-04213-9.
- [5] Manjunatha R, Schechter A. Electrochemical synthesis of ammonia using ruthenium–platinum alloy at ambient pressure and low temperature. *Electrochem. Commun.* **2018**, *90*:96–100. doi:10.1016/j.elecom.2018.04.008.
- [6] Lee HK, Koh CSL, Lee YH, Liu C, Phang IY, Han X, et al. Favoring the unfavored: Selective electrochemical nitrogen fixation using a reticular chemistry approach. *Sci. Adv.* **2018**, *4*:eaar3208. doi:10.1126/sciadv.aar3208.
- [7] Kong J, Lim A, Yoon C, Jang JH, Ham HC, Han J, et al. Electrochemical Synthesis of NH₃ at Low Temperature and Atmospheric Pressure Using a γ -Fe₂O₃ Catalyst. *ACS Sustain. Chem. Eng.* **2017**, *5*:10986–95. doi:10.1021/acssuschemeng.7b02890.
- [8] Chen S, Perathoner S, Ampelli C, Mebrahtu C, Su D, Centi G. Room-Temperature Electrocatalytic Synthesis of NH₃ from H₂O and N₂ in a Gas–Liquid–Solid Three-Phase Reactor. *ACS Sustain. Chem. Eng.* **2017**, *5*:7393–400. doi:10.1021/acssuschemeng.7b01742.
- [9] Zhou F, Azofra LM, Ali M, Kar M, Simonov AN, McDonnell-Worth C, et al. Electro-synthesis of ammonia from nitrogen at ambient temperature and pressure in ionic liquids. *Energy Environ. Sci.* **2017**, *10*:2516–20. doi:10.1039/C7EE02716H.
- [10] Zhang Y, Qiu W, Ma Y, Luo Y, Tian Z, Cui G, et al. High-Performance Electrohydrogenation of N₂ to NH₃ Catalyzed by Multishelled Hollow Cr₂O₃ Microspheres under Ambient Conditions. *ACS Catal.* **2018**, *8*:8540–4. doi:10.1021/acscatal.8b02311.
- [11] Xu G, Liu R, Wang J. Electrochemical synthesis of ammonia using a cell with a Nafion membrane and SmFe_{0.7}Cu_{0.3-x}Ni_xO₃ (x = 0-0.3) cathode at atmospheric pressure and lower temperature. *Sci. China, Ser. B Chem.* **2009**, *52*:1171–5. doi:10.1007/s11426-009-0135-7.
- [12] Zhang L, Ji X, Ren X, Luo Y, Shi X, Asiri AM, et al. Efficient Electrochemical N₂ Reduction to NH₃ on MoN Nanosheets Array under Ambient Conditions. *ACS Sustain. Chem. Eng.* **2018**:acssuschemeng.8b01438. doi:10.1021/acssuschemeng.8b01438.
- [13] Zhang R, Zhang Y, Ren X, Cui G, Asiri AM, Zheng B, et al. High-Efficiency Electrosynthesis of Ammonia with High Selectivity under Ambient Conditions Enabled by VN Nanosheet Array. *ACS Sustain. Chem. Eng.* **2018**, *6*:9545–9. doi:10.1021/acssuschemeng.8b01261.
- [14] Furuya N, Yoshida H. Electroreduction of nitrogen to ammonia on gas-diffusion electrodes loaded with inorganic catalyst. *J. Electroanal. Chem.* **1990**, *291*:269–72.
- [15] Lv C, Qian Y, Yan C, Ding Y, Liu Y, Chen G, et al. Defect Engineering Metal-Free Polymeric Carbon Nitride Electrocatalyst for Effective Nitrogen Fixation under Ambient Conditions. *Angew. Chemie Int. Ed.* **2018**, *57*:10246–50. doi:10.1002/anie.201806386.

- [16] Liu Y, Su Y, Quan X, Fan X, Chen S, Yu H, et al. Facile Ammonia Synthesis from Electrocatalytic N₂ Reduction under Ambient Conditions on N-Doped Porous Carbon. *ACS Catal.* **2018**, *8*:1186–91. doi:10.1021/acscatal.7b02165.
- [17] Mukherjee S, Cullen DA, Karakalos S, Liu K, Zhang H, Zhao S, et al. Metal-organic framework-derived nitrogen-doped highly disordered carbon for electrochemical ammonia synthesis using N₂ and H₂O in alkaline electrolytes. *Nano Energy* **2018**, *48*:217–26. doi:10.1016/j.nanoen.2018.03.059.
- [18] Yu X, Han P, Wei Z, Huang L, Gu Z, Peng S, et al. Boron-Doped Graphene for Electrocatalytic N₂ Reduction. *Joule* **2018**, *2*:1–13. doi:10.1016/j.joule.2018.06.007.
- [19] Song Y, Johnson D, Peng R, Hensley DK, Bonnesen P V., Liang L, et al. A physical catalyst for the electrolysis of nitrogen to ammonia. *Sci. Adv.* **2018**, *4*:e1700336. doi:10.1126/sciadv.1700336.
- [20] Ozin GA, Wang H, Wang L, Wang Q, Ye S, Sun W, et al. Ambient Electro-Synthesis of Ammonia-Electrode Porosity and Composition Engineering. *Angew. Chemie Int. Ed.* **2018**. doi:10.1002/anie.201805514.
- [21] Tsuneto A, Kudo A, Sakata T. Lithium-mediated electrochemical reduction of high pressure N₂ to NH₃. *J. Electroanal. Chem.* **1994**, *367*:183–8. doi:10.1016/0022-0728(93)03025-K.
- [22] McEnaney JM, Singh AR, Schwalbe JA, Kibsgaard J, Lin JC, Cargnello M, et al. Ammonia synthesis from N₂ and H₂O using a lithium cycling electrification strategy at atmospheric pressure. *Energy Environ. Sci.* **2017**, *10*:1621–30. doi:10.1039/C7EE01126A.
- [23] Kim K, Lee SJ, Kim D-Y, Yoo C-Y, Choi JW, Kim J-N, et al. Electrochemical Synthesis of Ammonia from Water and Nitrogen: A Lithium-Mediated Approach Using Lithium-Ion Conducting Glass Ceramics. *ChemSusChem* **2018**, *11*:120–4. doi:10.1002/cssc.201701975.
- [24] Ma J-L, Bao D, Shi M-M, Yan J-M, Zhang X-B. Reversible Nitrogen Fixation Based on a Rechargeable Lithium-Nitrogen Battery for Energy Storage. *Chem* **2017**, *2*:525–32. doi:10.1016/j.chempr.2017.03.016.
- [25] Shapiro I, Weiss HG. Preparation of Lithium Fluoborate. *J. Am. Chem. Soc.* **1953**, *75*:1753–4. doi:10.1021/ja01103a526.
- [26] Dabundo R, Lehmann MF, Treibergs L, Tobias CR, Altabet MA, Moisander PH, et al. The Contamination of Commercial ¹⁵N₂ Gas Stocks with ¹⁵N-Labeled Nitrate and Ammonium and Consequences for Nitrogen Fixation Measurements. *PLoS One* **2014**, *9*:e110335. doi:10.1371/journal.pone.0110335.
- [27] Verdouw H, Van Echteld CJA, Dekkers EMJ. Ammonia determination based on indophenol formation with sodium salicylate. *Water Res.* **1978**, *12*:399–402. doi:10.1016/0043-1354(78)90107-0.
- [28] Greenlee LF, Renner JN, Foster SL. The Use of Controls for Consistent and Accurate Measurements of Electrocatalytic Ammonia Synthesis from Dinitrogen. *ACS Catal.* **2018**, *8*:7820–7. doi:10.1021/acscatal.8b02120.
- [29] Connelly NG, Geiger WE. Chemical redox agents for organometallic chemistry. *Chem. Rev.* **1996**, *96*:877–910. doi:10.1021/cr940053x.
- [30] Dyre JC. Rayleigh scattering revisited. *Nat. Mater.* **2016**, *15*:1150–1. doi:10.1038/nmat4735.
- [31] Clark EL, Resasco J, Landers A, Lin J, Chung L-T, Walton A, et al. Data Acquisition Protocols and Reporting Standards for Studies of the Electrochemical Reduction of Carbon Dioxide. *ACS Catal.* **2018**:acscatal.8b01340. doi:10.1021/acscatal.8b01340.
- [32] Atkins P. Physical Chemistry. 6th Editio. New York: W.H. Freeman and Company; **1998**.

- [33] Wang Y, Rogers EI, Compton RG. The measurement of the diffusion coefficients of ferrocene and ferrocenium and their temperature dependence in acetonitrile using double potential step microdisk electrode chronoamperometry. *J. Electroanal. Chem.* **2010**, *648*:15–9. doi:10.1016/j.jelechem.2010.07.006.
- [34] Prem Kumar T, Prabhu PVSS, Srivastava AK, Bejoy Kumar U, Ranganathan R, Gangadharan R. Conductivity and viscosity studies of dimethyl sulfoxide (DMSO)-based electrolyte solutions at 25 °C. *J. Power Sources* **1994**, *50*:283–94. doi:10.1016/0378-7753(94)01911-8.
- [35] Littel RJ, Versteeg GF, van Swaaij WPM. Diffusivity Measurements in Some Organic Solvents by a Gas-Liquid Diaphragm cell. *J. Chem. Eng. Data* **1992**, *37*:42–5. doi:10.1021/je00005a014.
- [36] Pfeiffer WF, Krieger IM. Bubble Solution Method for Diffusion Coefficient Measurements. An Experimental Evaluation. *J. Phys. Chem.* **1974**, *78*:2516–21. doi:10.1021/j100617a019.
- [37] Cadogan SP, Maitland GC, Trusler JPM. Diffusion Coefficients of CO₂ and N₂ in Water at Temperatures between 298.15 K and 423.15 K at Pressures up to 45 MPa. *J. Chem. Eng. Data* **2014**, *59*:519–25. doi:10.1021/je401008s.
- [38] Kretschmer CB, Nowakowska J, Wiebe R. Solubility of Oxygen and Nitrogen in Organic Solvents from –25° to 50° C. *Ind. Eng. Chem.* **1946**, *38*:506–9. doi:10.1021/ie50437a018.
- [39] Gibanel F, López MC, Royo FM, Santafé J, Urieta JS. Solubility of nonpolar gases in tetrahydrofuran at 0 to 30°C and 101.33 kPa partial pressure of gas. *J. Solution Chem.* **1993**, *22*:211–7. doi:10.1007/BF00649244.
- [40] Weisenberger S, Schumpe A. Estimation of Gas Solubilities in Salt Solutions at Temperatures from 273 K to 363 K. *AIChE J.* **1996**, *42*:298–300. doi:10.1002/aic.690420130.
- [41] Gittleson FS, Jones RE, Ward DK, Foster ME. Oxygen solubility and transport in Li-air battery electrolytes: Establishing criteria and strategies for electrolyte design. *Energy Environ. Sci.* **2017**, *10*:1167–79. doi:10.1039/c6ee02915a.
- [42] Bard AJ, Faulkner LR. *Electrochemical Methods. Fundamentals and Applications*. 2nd Editio. Phoenix: John Wiley & Sons, Inc; **2001**.